2023

An appraisal of tornado-induced load provisions in ASCE/SEI 7-22 and 7-16 for residential low-rise buildings.

Gabriel Narancio
Western University, enaranci@uwo.ca

Djordje Romanic

Jubayer Chowdury

Han-Ping Hong

Horia Hangan

An appraisal of tornado-induced load provisions in ASCE/SEI 7-22 and 7-16 for residential low-rise buildings.

Gabriel Narancio[a,*], Djordje Romanic[a], Jubayer Chowdhury[a], Han-Ping Hong[b], Horia Hangan[a]

[a] *WindEEE Research Institute, Western University, 2535 Advanced Ave, London, N6M 0E2, ON, Canada*
[b] *Department of Civil and Environmental Engineering, Western University, Spencer Engineering Building, London, N6A 5B9, ON, Canada*

Abstract

In this study, the loads induced by tornado-like vortices on scaled models of eight low-rise residential buildings with real-world shapes in a typical North American community are quantified and compared to the provisions provided by ASCE/SEI 7-16 and 7-22. Physical simulations of the interaction between translating tornado-like vortices representative of EF1-, EF2- and EF3-rated tornadoes and the scaled models were performed in the WindEEE Dome at the University of Western Ontario. Three internal pressure scenarios were numerically simulated. The tornado velocity gust factor was identified as a critical parameter when translating loads from model to full-scale. The load comparison results show that the provisions are safer as the rating of the design tornado increases. The uplift forces on the whole roof in the internal pressure scenarios with one dominant opening are between 44% and 63% higher than the distributed leakage scenario, highlighting the importance of keeping the integrity of the envelope. The ratios of pressures obtained from physical simulation to the ones calculated using the standard are higher on the walls than on the roof. Pressure ratios on the eaves are higher than on other parts of the roof.

Keywords: Tornado, Wind loads, Physical simulation, Low-rise buildings, Tornado-resistant design, Internal pressure, ASCE/SEI 7-22, ASCE/SEI 7-16

Nomenclature

Acronyms

*Corresponding author
Email address: enaranci@uwo.ca (Gabriel Narancio)

ABL Atmospheric Boundary Layer

APD Atmospheric Pressure Deficit

ASCE/SEI American Society of Civil Engineers/Structural Engineering Institute

ASHRAE The American Society of Heating, Refrigerating and Air-Conditioning Engineers

C&C Components & Cladding

DI Damage Indicator

DOD Degree Of Damage

DTC Digital Temperature Compensation

EF Enhanced Fujita Scale

EPS Electronic Pressure Scanners

EWA Effective Wind Area

GEVD Generalized Extreme Value Distribution

MDE Multiple Discharge Equations

MWFRS Main Wind Force Resisting System

RMW Radius of Maximum Wind

TFI Turbulent Flow Instrumentation Pty Ltd.

TLV Tornado Like Vortex

TVG Tornado Vortex Generator

UMS University Machine Services

USA United States of America

WindEEE The Wind Engineering, Energy and Environment

Symbols

α Significance level

$\ddot{x}_j$ Flow acceleration through the opening assigned to tap j

$\dot{x}_j$ Flow velocity through the opening assigned to tap j

ℓ_{ej} Effective length at the opening assigned to tap j

ϵ_j Envelope porosity at the tributary area of tap j

γ Heat capacity ratio of air

Γ_∞ Background circulation

$\hat{u}\,(t, T)$ Peak value of the moving average velocity with a window width t in the period T

λ_L Geometric scale

λ_T Time scale

λ_V Velocity scale

$\mathbf{F}$ Force

$\mathcal{S}$ Swirl ratio

f Sampling frequency

μ Population mean

$\overline{U}$ Mean velocity

$\overline{x}$ Sample mean

ρ Air density

σ^2 Population variance

$\mathbf{n}_j$ Unit normal vector at tap j

a Width of the pressure coefficient zone

A_j Tributary area assigned to tap j

C_F Force coefficient

C_p External pressure coefficient

C_{pi} Internal pressure coefficient

C_{pref} External pressure coefficients used for the standard calculation

Dt Time step of internal pressure simulation

F_x, F_y, F_z Components of the overall force along x,y, and z

G Gust-effect factor

G_T Gust-effect factor for tornadoes

$G_{vTor,ref}$ Tornado velocity gust factor used here to report ratios r_{ref}

G_{vTor} Tornado velocity gust factor

h Mean roof height of a building

k Discharge coefficient at the opening assigned to tap j

K_d Directionality factor

K_e Elevation factor

K_h Exposure factor at height h

K_z Exposure factor

K_{dT} Directionality factor for tornadoes

K_{vT} External pressure coefficient adjustment factor for vertical winds

K_{zT} Tornado exposure coefficient

K_{zt} Topographic effect factor

n Flow exponent at the opening assigned to tap j

p_j Pressure at tap j

Q Incoming flow rate

q Velocity pressure

q_h Velocity pressure evaluated at z=h

q_i Velocity pressure for internal pressure determination

r Ratio between loads calculated from physical simulations and calculated from the standards

r_0 Radius of the convergence zone

$r_{c,max}$ Radius to the average maximum tangential wind speed

r_{ref} Reference ratio reported

S^2 Sample variance

Tol Maximum tolerance between iterations

V Design wind speed

V_T Design tornado wind speed

$V_{3s,max,i}$ Maximum 3-second equivalent gust velocity in segment i

$V_{mean,i}$ Average velocity in segment i

$V_{o,FS}$ Full-scale volume of the building

$V_{o,MS}$ Scaled volume the model building

$V_{tan,max,o}$ Average maximum tangential wind speed

w_s 3-second equivalent window in samples

w_t 3-second equivalent window in time units

x, y, z House fixed coordinate system with x along the ridge, y perpendicular to the ridge and z, vertical

z_{max} Vertical position of the average maximum tangential wind speed

Subscripts

$ASCE$ Found from calculations using ASCE/SEI 7-16 or 7-22 standards

FS Full-scale

int Internal

M Model

MS Model scale

$WindEEE$ Found from physical simulations at the WindEEE Dome

1. Introduction

Tornado wind loads were not specified in building codes for a long time despite generating extensive damage and loss of life in many parts of the world (Grazulis, 2001), notably in the United States of America (USA), where they cause roughly twice as much loss as earthquakes and half as much as hurricanes (Simmons et al., 2013). This omission was justified in ASCE/SEI 7-16 by the low probability of occurrence of tornadoes (ASCE, 2017); however, the latest edition of the standard (ASCE/SEI 7-22) states that "recent research on tornado climatology has shown that tornadoes occur with much greater frequency and intensity than had previously been quantified" which is the reason for the addition of a full chapter on tornado resistant design in ASCE/SEI 7-22 (ASCE, 2022). Moreover, tornado hazard mappings for the USA and Canada have been reported by Twisdale et al. (2021) and Hong et al. (2021).

Additionally to the evidence that tornadoes occur more frequently than thought, a careful analysis of tornado damage records and the associated wind levels has indicated that most tornado damage is induced by tornadoes rated 3 or lower in the Enhanced Fujita (EF) Scale (Simmons et al., 2013). Furthermore, EF ratings are assigned according to the maximum velocity inferred from the Degrees Of Damage (DOD) observed in Damage Indicators (DI), which means that most of the damaged area is caused by lower-intensity winds. For example, the Tuscaloosa (2011) tornado rated EF4 had only 2.7% of the damaged area rated as EF4, the other 97.3% was EF0-EF3 damage (Prevatt et al., 2012). The wind speed associated with EF0-EF3 is comparable to hurricane winds for which ASCE 7 has had provisions for decades and mitigation measures have been implemented. These observations led van de Lindt et al. (2013) to propose a dual-objective-based approach to design for tornadoes that considers reducing damage for tornadoes rated EF3 or lower and minimizing the loss of life for high-end EF4- or EF5-rated tornadoes.

The current understanding of tornado-induced loads is limited when compared to Atmospheric Boundary Layer (ABL) induced loads for which the conventional ABL wind tunnel technique is mature. The recent relative proliferation of Tornado Vortex Generators (TVG) designed for wind engineering applications (Haan Jr et al., 2008; Mayer, 2009; Zhang and Sarkar, 2009; Sabareesh et al., 2012; Hangan, 2014; Wang et al., 2017; Gillmeier et al., 2018), has allowed for a better comprehension of tornado-induced loads and some quantitative knowledge.

The loading effect of Tornado-like Vortices (TLVs) on low-rise buildings has been investigated by several researchers employing physical simulation (Jischke and Light, 1983; Bienkiewicz and Dudhia, 1993; Mishra et al., 2008; Sengupta et al., 2008; Haan Jr et al., 2010; Hu et al., 2011; Case et al., 2014; Haan Jr, 2017; Wang et al., 2018; Razavi and Sarkar, 2018; Sabareesh et al., 2018; Roueche et al., 2020; Kopp and Wu, 2020; Wang et al., 2020; Wang and Cao, 2021; Razavi and Sarkar, 2021; Williams and Dragomirescu, 2023). There is considerable agreement that the pressure distribution patterns induced by tornadoes and straight-line winds on low-rise buildings are different due to the three-dimensional nature and curvature of tornado flow. There is less agreement on the load values. The reported values of the tornado-induced to straight-line-induced pressure coefficient ratios range from 1 to 5.

Most past studies have focused on isolated buildings. Only a few have considered the effect of multiple buildings and their sheltering effect e.g. Zhang and Sarkar (2009) and Sabareesh et al. (2018). They concluded that lateral forces can be reduced by the presence of adjacent buildings but the uplift force can decrease or increase without a clear pattern.

Case et al. (2014) analyzed the effect of low-rise building geometry on tornado-induced loads and found that the loads depend on "eave height, roof pitch, aspect ratio, plan area, and other differences in geometry such as the addition of a garage and modeling of the roof overhang and soffit". No study has analyzed the loading on residential low-rise buildings with complex roof configurations and plan shapes. All studies have considered simple gable roof buildings.

Tornadoes induce a pressure deficit around their core that has no counterpart in straight-line winds. This depression, usually termed Atmospheric Pressure Deficit (APD) (Roueche et al., 2020), develops as the flow needs a radial pressure gradient to balance centrifugal forces. The building's internal pressure behavior depends on the APD, the capacity of the building to respond to atmospheric pressure changes, and the presence of large openings in the envelope. Therefore, measuring or modeling internal pressure is critical, even more so than in ABL flows. Some researchers have included an internal pressure model (Roueche et al., 2020) or direct measurements (Wang et al., 2020) in their evaluation of tornadic loads. For straight-line winds, it has been established that the use of the Multiple Discharge Equations (MDE) for internal pressure modeling can lead to accurate estimates of the internal pressure time series based on external pressures, even capturing the Helmholtz resonant peak (Oh et al., 2007). The question of whether the models used for internal pressure under straight-line winds are as effective when used to predict internal pressure under tornado wind was addressed by Jaffe and Kopp (2021). They found that the MDE model reasonably reproduces internal pressures but with lower accuracy than under straight-line winds which can be explained by the presence of sub-vortices and the vertical component of the wind velocity.

In December 2021, an updated ASCE/SEI 7-22 Minimum Design Loads and Associated Criteria for Buildings and Other Structures was released. This standard included a chapter (Chapter 32) on tornado-resistant design for buildings in Risk Categories III and IV in tornado-prone areas (ASCE, 2022). This is the first standard to include provisions for tornado-induced loads. ASCE/SEI 7-16 (ASCE, 2017) provided design guidance for tornadoes to reduce damage caused by EF0- to EF2-rated tornadoes or increase occupant protection but it wasn't mandatory. The guidance from ASCE/SEI 7-16 was only for owners who wanted to have a higher level of safety on their property even knowing that designing for tornadoes implies a much higher design return period than typically used for residential buildings.

ASCE/SEI 7-16 and 7-22 have important differences in the way tornado-induced loads are calculated. These include:

- In ASCE/SEI 7-22, the tornado design wind speed is the expected tornado velocity with 1700 and 3000-year return periods for Risk Categories III and IV respectively, which depend on the plan area. In ASCE/SEI 7-16 the design wind speed was the upper end-of-range for the tornado rating being considered for design.
- The Simplified and Extended method's in ASCE/SEI 7-16 are no longer used in ASCE/SEI 7-22.
- In ASCE/SEI 7-22, the directionality factor depends on the structure type. In ASCE/SEI 7-16 it was 1.0.
- The exposure coefficient in ASCE/SEI 7-22 decreases with height as opposed to ASCE/SEI 7-16 in which increased.
- The enclosure classification in ASCE/SEI 7-22 is done considering each wall as a windward wall.
- If the glazed openings are not required to be protected, the building shall be evaluated as a partially enclosed building in ASCE/SEI 7-22.
- Internal pressure coefficients are the same in ASCE/SEI 7-16 and 7-22 except for the addition, in ASCE/SEI 7-22, of the Sealed enclosure classification for which the internal pressure coefficient is +1.0.

- An external pressure coefficient adjustment factor for vertical winds (K_{vT}) is introduced in ASCE/SEI 7-22. This factor corrects the pressure coefficient obtained from Chapters 27 and 30 in both ASCE/SEI 7-16 and 7-22, for the increased vertical angle of attack.

Provisions in ASCE/SEI 7-22 are based on the hypothesis that the loads induced by tornadoes can be calculated using ABL wind tunnel-obtained pressure coefficients. The pressure coefficients are then corrected by the factor that accounts for the change in the vertical angle of attack K_{vT}. This hypothesis has not been extensively tested.

The scope of Chapter 32 of ASCE/SEI 7-22 is limited to buildings in Risk Category III or IV located in tornado-prone areas, therefore, residential low-rise buildings are excluded. Despite this, its publication presents a good opportunity to evaluate the performance of residential low-rise buildings designed following its provisions.

This research aims to quantify the expected maximum loads on residential low-rise buildings subjected to tornado loading and compare them to the design loads provided by ASCE/SEI 7-16 and 22 for tornadoes. For this, the loads induced by several translating TLVs generated in the WindEEE Dome at the University of Western Ontario (UWO) representatives of EF1-, EF2-, and EF3-rated tornadoes, on a model of a part of the community of Dunrobin, Ontario, Canada, which was affected by a tornado on September 2018, are compared to both ASCE/SEI 7-16 guidance and ASCE/SEI 7-22 provisions. The model includes eight low-rise residential buildings with different real-world roof geometries i.e. gable, hip, hip and valley, and dormer roofs representing a typical North American wood-frame residential community. Different scenarios in terms of internal pressure are simulated using the MDE model.

2. Experimental setup

2.1. Physical simulations

The physical simulations that are presented in this research were performed at the Wind Engineering, Energy, and Environment (WindEEE) Dome at the UWO, Canada. The WindEEE Dome is a novel wind testing chamber capable of modeling a wide range of three-dimensional and time-dependent atmospheric flows, with a focus on wind engineering, wind energy, and environmental problems as its name implies. Specifically, the facility is aimed at

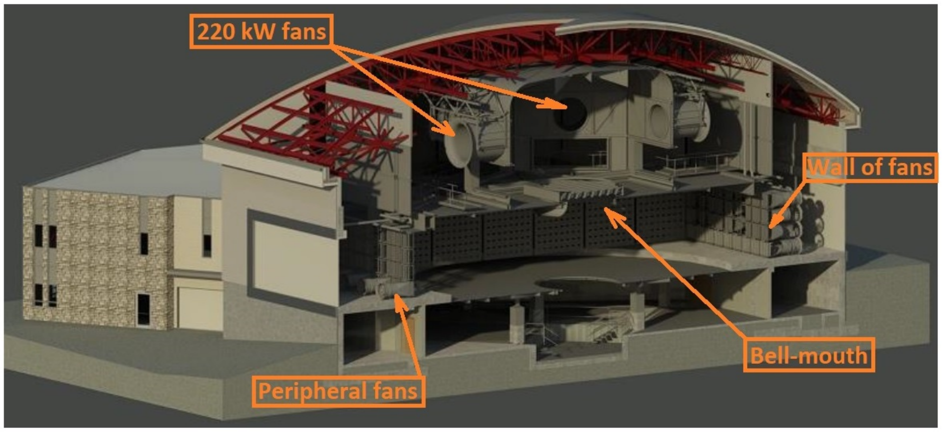

Fig 1. WindEEE Dome section showing the main parts.

reproducing tornadoes, downbursts, gusts and currents, shear flows, and boundary layer flow at high Reynolds numbers (Hangan et al., 2017).

The main chamber is hexagonal with a diameter of 25m. This chamber is surrounded by a hexagonal return chamber 40m in diameter. On the periphery of the main chamber, there are 100 30kW fans of which 60 are located on one lateral wall in 4 rows by 15 columns arrangement. On the ceiling, a mobile bell mouth communicates between the main chamber and the upper plenum where 6x220kW fans can generate flow into or out of the main chamber. The mobile bell-mouth allows for the simulation of translating TLVs and downbursts. A section of the facility is shown in Fig. 1.

There are two modes of operation to produce TLVs: Modes A and B. In Mode A only the fans in the upper plenum operate in suction mode and the circulation is created by inducing a tangential component to the returning flow using directional louvers (Refan and Hangan, 2018). The scale of the TLVs is enhanced in Mode B operation by activating the peripheral fans (Ashrafi et al., 2021).

2.2. The Wind Flow

The flow characteristics in TLVs are controlled by the swirl ratio

$$\mathcal{S} = \frac{r_0 \Gamma_\infty}{2Q}, \tag{1}$$

the aspect ratio and only weakly by the Reynolds number. In Eq. (1), Q is the incoming flow rate, r_0 is the radius of the convergence zone and Γ_∞ is the background circulation. The

Table 1

Characteristics of the TLVs generated in Mode A.

S	$V_{tan,max,o}$ ($^m/_s$)	$r_{c,max}$ (m)	z_{max} (m)	EF-rating	λ_L	λ_v
0.21	8.8	0.27	0.2	-	-	-
0.48	11.5	0.45	0.2	EF1	160-300	-
0.59	12.8	0.42	0.2	-	-	-
0.76	13.8	0.60	0.2	EF2	200-280	∼2.1
1.03	16.2	0.69	0.2	EF3	200-280	∼2.1

swirl ratio is a measure of the relative spin of the tornado to the radial velocity. It has been shown that the structure of TLVs changes as the swirl ratio increases, from a single laminar vortex ($\mathcal{S} < 0.2$), a single vortex with breakdown ($0.2 < \mathcal{S} < 0.4$), two interlocking spiral vortices ($0.4 < \mathcal{S} < 1.0$) and more than one subsidiary vortex ($1.0 < \mathcal{S}$) (Church et al., 1979; Karami et al., 2019).

All TLVs in this research were generated using Mode A. The flow characteristics of these TLVs were investigated by Refan and Hangan (2018). The reader is referred to the cited article for details on the flow characteristics. A summary of the most important parameters of the TLVs generated in Mode A is presented in Table 1. In Table 1, $V_{tan,max,o}$ is the average maximum tangential wind speed, $r_{c,max}$ is the radius to the maximum tangential wind speed, z_{max} is the vertical location of the same wind speed, λ_L is the geometric scale and λ_v is the velocity scale.

TLVs with swirl ratios $\mathcal{S} = 0.48, \quad 0.76$, and 1.03 are shown to match reasonably the characteristics of EF1-, EF2-, and EF3-rated tornadoes with geometric scales between 160 and 300. It is important to note that the characteristics of TLVs were studied for the stationary case, therefore, for the translating case, it is assumed that the characteristics are unchanged for the same hardware set-up only adding a constant translation velocity component.

2.3. Model and measurements

As mentioned before, a neighborhood in Dunrobin, Ontario that was affected by the passage of the September 21, 2018, EF3-rated tornado was used as an example of a typical

(a)

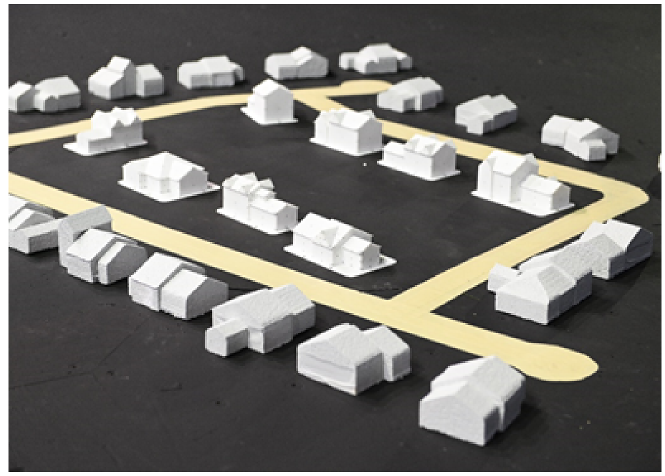

(b)

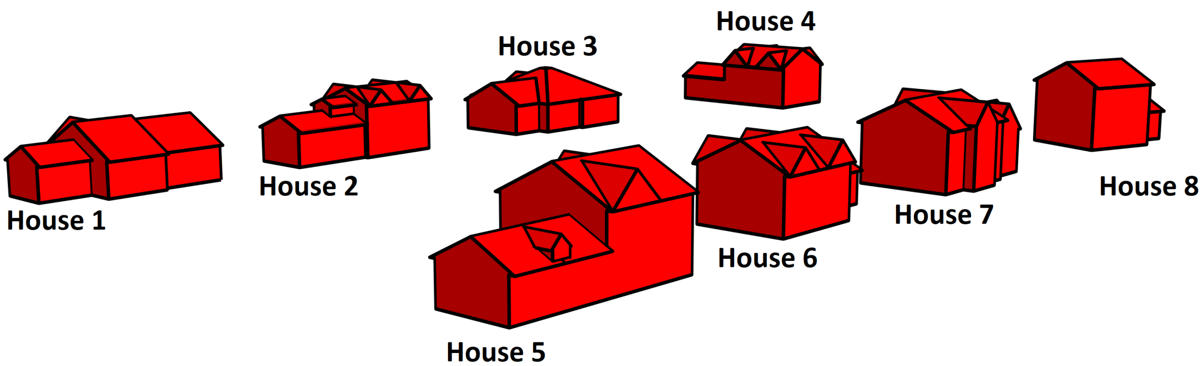

(c)

Fig 2. Dunrobin model, (a) satellite view of the Dunrobin community in May 2015 (Image taken from Google Earth™), (b) Model, (c) House numbering.

North American residential community.

The scaled model of the community consists of 8 instrumented residential low-rise buildings with 22 non-instrumented surrounding buildings at a 1:150 geometric scale (see Fig. 2b). The instrumented houses are located inside the near rectangular shape delimited by the roads in Fig. 2a.

The scaled models were 3D-printed at UWO's Machine Services (UMS). The total number of pressure taps was 1152 distributed in the 8 instrumented houses and on the ground plate. Each house had an average of 120 pressure taps.

The pressure measurement system consists of miniature Electronic Pressure Scanners (EPS) coupled with Digital Temperature Compensation (DTC) Initiums. The pressure scanners used in this study are ESP-32HD manufactured by Pressure Systems, Inc. (PSI) which have 32 scanning ports each. ESP Pressure Scanners are miniature electronic differential pressure measurement units consisting of an array of silicon piezoresistive pressure sensors, one for each pressure port. This device allows for measurement at frequencies up to 70,000 Hz per channel. The scanner's amplified analog output is then sampled at a remote A/D converter (DTC Initium). The DTC Initium is connected to the scanner via an Ethernet-based connection. The accuracy of the DTC Initium is ±0.05% over the entire operating temperature range ($0^o C$–$70^o C$).

The scanners are connected to the pressure taps using a tubing system that acts like a low pass filter attenuating the signal at frequencies higher than 210 Hz, the cut-off frequency of the filter. To eliminate aliasing from the pressure signal, the sampling frequency is set at 500 Hz, higher than two times the cut-off frequency of the low pass filter (Nyquist rate).

The wind velocity measurements were performed using four Cobra Probes from Turbulent Flow Instrumentation Pty Ltd. (TFI). The system of cobra probes located one radius of maximum wind (RMW) away from the path of the simulated tornado was synchronized to the pressure measurement system. The 4-hole differential pressure Cobra Probes can measure the three components of the velocity and local pressure at frequencies lower than 2000 Hz. These probes can correctly resolve the components of the wind velocity only when the angle between the wind velocity vector and the probe x-axis is less than 45^o. The analog output is then read by an A/D converter. The velocity components are calculated using proprietary acquisition software. The manufacturer claims that the Cobra Probes need no additional calibration other than the factory calibration.

Table 2 shows the parameters of the 17 different configurations tested. Three cases (W3E13, W3E14, and W3E15) involve stationary TLVs corresponding to EF1-, EF2-, and EF3-rated tornadoes which are centered on the model table (see Fig. 3). In the other 14 cases, the TLVs translate along a quasi-straight line path. Two translating directions were selected: (1) 80^o from North clockwise, which represents the actual path of the 2018 Dunrobin tornado, and (2) 45^o which is the most probable orientation for strong tornadoes (Romanic et al., 2016). For each direction, EF1-, EF2-, and EF3-rated TLVs were simulated with two offsets from the center: (1) zero and (2) one RMW. Two more translating EF3-rated tornadoes were simulated at both mentioned translating directions with an offset of 2RMW, to consider the uncertainty of the actual location of the Dunrobin tornado path. Fig. 3 shows the paths of the translating TLVs. The central path (orange) in both sub-figures is shared by EF1-, EF2- and EF3-rated TLVs.

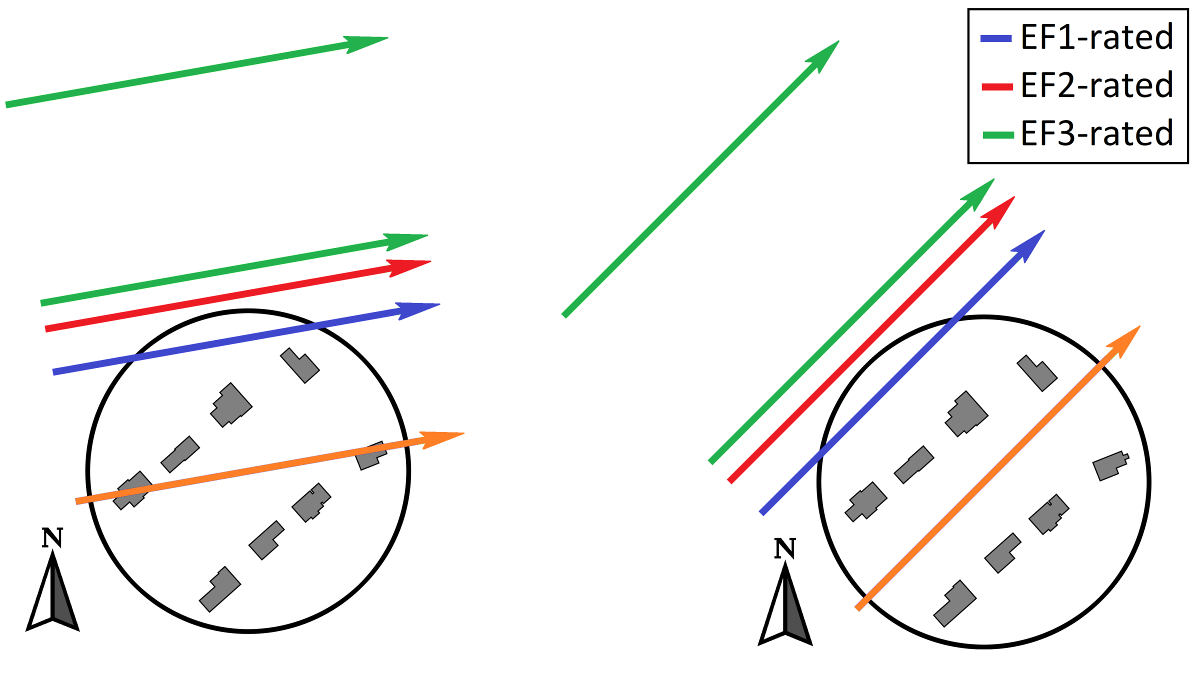

(a) (b)

Fig 3. Translating TLVs paths. (a) 80^o degrees clockwise from North (b) 45^o degrees clockwise from North

The translation speed of all TLVs was fixed at 1.3 $^m/_s$. The case with EF3-rated TLV and zero offsets was repeated 10 times. All other translating TLVs were repeated 5 times. The sampling time for translating TLVs was 60 s and 120s for the stationary TLVs.

3. Procedure

The applicability of the procedures in both ASCE/SEI 7-16 and 7-22 is restricted to "regular shape" buildings. Most residential low-rise buildings don't fit exactly into this definition. It is common to see L, T, and other plan shapes; hip and valley, dormer, cross-hipped, intersecting roofs, and more. Despite this, the standard recognizes the practical necessity to balance the range of applicability between situations that are outside but reasonably close to the "regular shape" building archetype, while restricting the use for clearly unusual shapes

Table 2

Parameters of the studied cases.

Case code	Tornado	Offset	Angle	Movement	Number of runs	Sampling time (s)
W3E1	EF3	0	80	Translation	10	60
W3E2	EF3	0	45	Translation	5	60
W3E3	EF2	0	45	Translation	5	60
W3E4	EF2	0	80	Translation	5	60
W3E5	EF1	0	80	Translation	5	60
W3E6	EF1	0	45	Translation	5	60
W3E7	EF1	+RMW	45	Translation	5	60
W3E8	EF1	+RMW	80	Translation	5	60
W3E9	EF2	+RMW	80	Translation	5	60
W3E10	EF2	+RMW	45	Translation	5	60
W3E11	EF3	+RMW	45	Translation	5	60
W3E12	EF3	+RMW	80	Translation	5	60
W3E13	EF3	0	-	Stationary	1	120
W3E14	EF2	0	-	Stationary	1	120
W3E15	EF1	0	-	Stationary	1	120
W3E16	EF3	+2RMW	80	Translation	5	60
W3E17	EF3	+2RMW	45	Translation	5	60

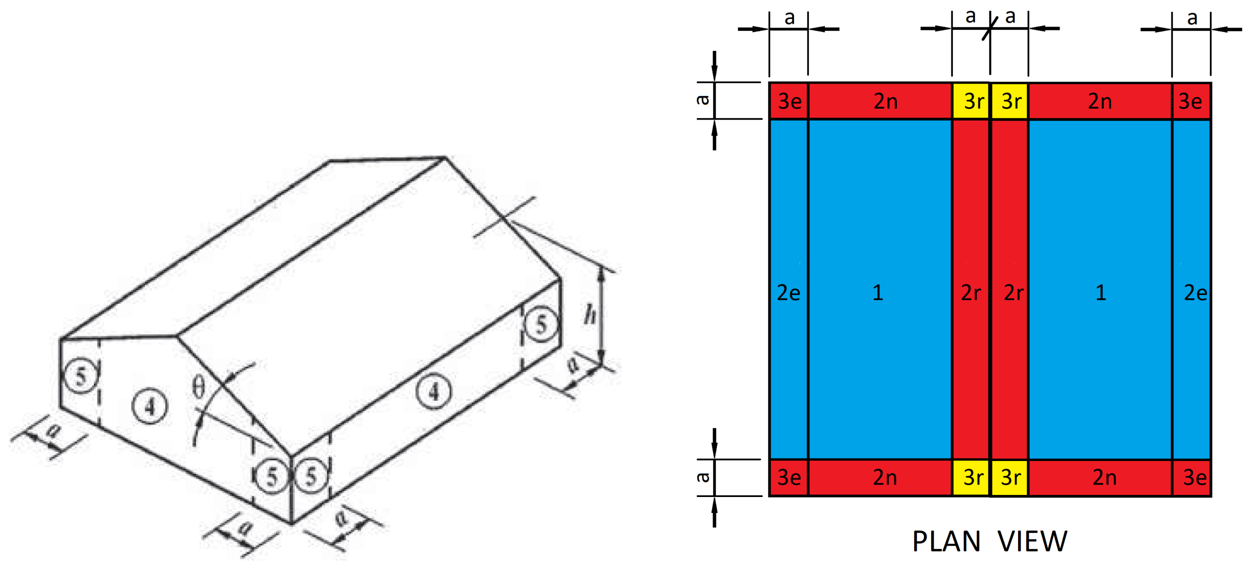

(a) (b)

Fig 4. Components & Cladding zones. (a) On the walls (b) on the roof (taken from ASCE/SEI 7-16, Chapter 30, Figures 20.3-1 and 30.3-2C)

which need wind tunnel testing. In addition, it is expected that the loads calculated using the pressure coefficients obtained from the simple archetypes of the standard to be conservative when applied to complicated shapes (ASCE, 2017). Accordingly, it is assumed that the provisions can be applied to the Dunrobin model houses.

The gable roof archetypes in ASCE/SEI 7-16 and 7-22, look like the one depicted in Fig. 4a. For the Components & Cladding (C&C) pressure comparison, only the part of the building that has a gable roof is considered. This can be better understood by observing Fig. 5a, which shows, in color, the part of the building used for the calculation of C&C pressure coefficients, the grey part is ignored.

To calculate overall forces for the Main Wind Force Resisting System (MWFRS), a virtual "envelope" gable-roof house is created from the outline of each building. The force on this virtual house is multiplied by the ratio of the actual plan area of the house to that of the virtual house. This concept is shown in Fig. 5b for House 1. Dormers are ignored. Also, House 3 is ignored since it has a large hip roof and therefore can't be fitted reasonably in a gable-roof envelope house.

For the MWFRS calculations, the pressure coefficients are extracted from Chapter 27,

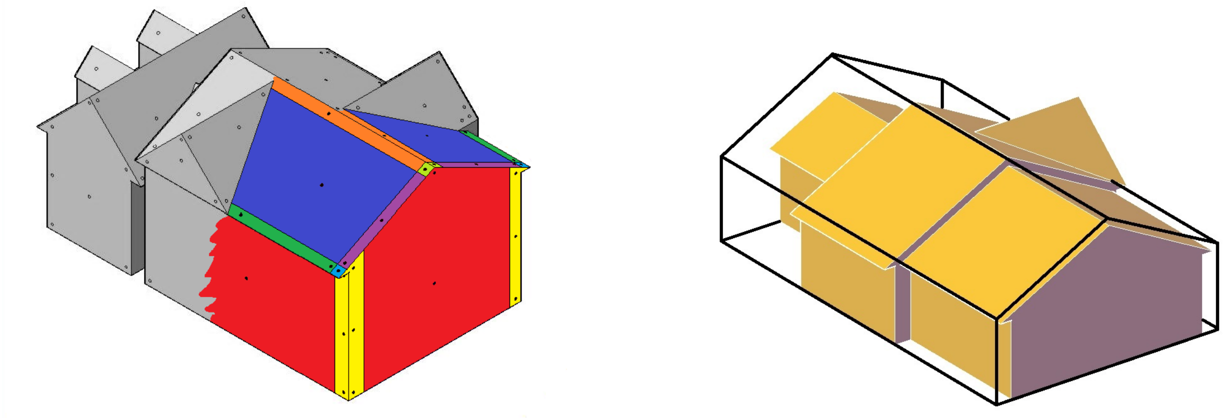

(a) (b)

Fig 5. (a) ASCE/SEI 7-16 Components & Cladding zones on House 7 (1-blue, 2e-green, 2n-purple, 2r-orange, 3e-light blue and 3r-light green) (b) envelope House 1 for MWFRS calculation.

Figure 27.3-1 in both ASCE/SEI 7-16 and 7-22, which are identical. For C&C, the pressure coefficients are obtained from Chapter 30, Figure 30.3-1 and Figures 30.3-2C, which have some minor differences in both standard editions, e.g. the roof zones in ASCE/SEI 7-16 that have the same pressure coefficient values are merged together in ASCE/SEI 7-22. Fig. 4b shows the zones in ASCE/SEI 7-16, named 1, 2e, 2n, 2r, 3e, 3r, 4, and 5, and in color, the merged zones in ASCE/SEI 7-22: (1) blue, (2) red and (3) yellow. In addition, the sloped part of the pressure coefficient plots on the roof is slightly modified in ASCE/SEI 7-22.

Since the pressure tap density is not high enough to allow for area-averaged pressure coefficient calculation around areas close to 10 ft^2 in full-scale, the comparison is performed for point pressure. This means that the pressure measured is not spatially averaged and the pressure coefficients for the code calculations are found from the horizontal part of the plots in Figures 30.3-1 and 30.3-2C in ASCE/SEI 7-16 and 7-22 at effective wind areas (EWA) lower than 10 fr^2. This will be further elaborated in Section 4.4.

3.1. ASCE/SEI 7-16 extended method

The design wind velocity (V) is the upper end-of-range corresponding to the desired EF rating. For example, if the goal is to design for EF3-rated tornadoes, the design 3-second wind gust speed should be 73.8 m/s. In line with the damage reduction design philosophy mentioned in Section 1, only EF1-, EF2-, and EF3-rated tornadoes are considered in this research. The upper end-of-range wind speed for each rating can be found in Table 3.

Table 3

EF scale velocity limits (3-second wind gust in m/s) (Marshall et al., 2004)

EF-scale	Lower speed limit (m/s)	Upper speed limit (m/s)
5	89.4	-
4	73.8	89.4
3	60.4	73.8
2	49.2	60.4
1	38.0	49.2
0	29.1	38.0

The calculation of the design pressure (p) is as follows:

$$p = q_h \left[GC_p - GC_{pi} \right] \tag{2}$$

where GC_p and GC_{pi} are the products of the gust-effect factor G and the external C_p and internal C_{pi} pressure coefficient respectively, and q_h is the velocity (or dynamic) pressure at height h, which is calculated as

$$q_h = 0.613 K_d K_h K_{zt} K_e V^2 \quad (Pa). \tag{3}$$

In Eq. (3), the directionality factor K_d, the topographic effect factor K_{zt} and the ground elevation factor K_e are all set to unity (see Section C26.14 in ASCE (2017). V is the design wind speed and the product GC_{pi} in Eq. (2) is ± 0.55.

ASCE/SEI 7-16 recommends assuming an exposure C and to use an exposure coefficient at the height of the building $K_z = K_h$. Since the buildings in the considered neighborhood have an average height close to $10m$, a $K_h = 1.0$ will be used.

The internal pressure coefficient value ± 0.55 used in Eq. (2) considers the fact that breaches in the envelope are highly probable during tornadoes due to the presence of flying debris. A breach in the envelope creates an opening that causes the internal pressure to increase (decrease) if the opening is on the windward (leeward) face. Accordingly, the same value used for the partially enclosed buildings under straight-line wind is used for the tornado's internal pressure.

ASCE/SEI 7-16 offers an alternative simplified method that won't be used here. The simplified method is formulated to make calculations easier in such a way that the designer can reuse the calculations done for straight-line winds. The idea is that the designer can calculate the provisions for straight-line winds in a particular location and then correct the results with the help of the so-called tornado factor which accounts for the uncertainty in the parameters. In ASCE/SEI 7-16, Chapter C26, it is shown that the results for both methods are equivalent (ASCE, 2017).

3.2. ASCE/SEI 7-22 design Provisions

As was explained in the Introduction, there are a few important differences, in the context of this article, between ASCE/SEI 7-22 and ASCE/SEI 7-16 i.e. the inclusion of a sealed building classification and the use of an external pressure coefficient adjustment factor for vertical winds, among others listed in Section 1.

The pressure calculation for MWFRS is performed in accordance with the following equations:

$$p = qG_T K_{dT} K_{vT} C_p - q_i \left(GC_{p_i}\right) \tag{4}$$

$$q = 0.613 K_{zT} K_e V_T^2 \quad (Pa) \tag{5}$$

where $q_i = q$, the directionality factor for tornadoes K_{dT}, the tornado exposure coefficient K_{zT} and the ground elevation factor K_e are all set to 1.0, the gust-effect factor for tornadoes is $G_T = 0.85$, V_T is the design tornado wind speed, the external pressure coefficient adjustment factor for vertical winds is $K_{vT} = 1.1$ and, as usual, C_p is the external pressure coefficient and GC_{p_i} is the product of the gust-effect factor and the internal pressure coefficient, which is +1.0 for Sealed classification and +0.55 for the Enclosed and Partially enclosed classification.

For C&C, the equations used are:

$$p = q_h \left[K_{dT} K_{vT} \left(GC_p\right) - \left(GC_{p_i}\right)\right] \tag{6}$$

and Eq. (5) with $q = q_h$. Now, $K_{dT} = 0.75$, the external pressure coefficient adjustment factor for vertical winds is $K_{vT} = 1.2$ for Zone 1, $K_{vT} = 1.2$ for Zone 2 and $K_{vT} = 1.3$ for Zone 3.

3.3. Physical simulation calculations (WindEEE Dome)

The forces on any part of each model house can be calculated by summing the contributions of each pressure tap on the surface of the building using Eq. (7).

$$\mathbf{F}_M(t) = -\sum_{j=1}^{N} \left[p_j(t) - p_{int}(t)\right] A_j \mathbf{n}_j \tag{7}$$

where the subscript M indicates force on the model, j is the identification number of the pressure taps from 1 to N, which is the total number of pressure taps that are involved in the calculation of the force, $p_j(t)$ is the time history of the pressure on tap j, $p_{int}(t)$ is the time history of the internal pressure for the house being considered, A_j is the tributary area assigned to tap j and $\mathbf{n}_j$ is the unit normal vector for each pressure tap.

The tributary area A_j is assigned to each pressure tap using a Voronoi tessellation (Burrough et al., 2015) for each face. As an example, Fig. 6 shows the tributary areas assigned to each pressure tap on House 2. The blue arrows indicate both the normals $\mathbf{n}_j$ to the surface and the location of the pressure taps.

The maximums of the force or pressure time histories, depending on the goal, are extracted from each run and fitted to a Gumbel distribution using Lieblein's BLUE method (Lieblein, 1976; Hong et al., 2013), as in Roueche et al. (2020). Fig. 7 shows the time histories of the three components of the overall force on House 5 in Case 1, Run 1, with a dominant opening (yellow square) in full-scale.

Due to the absence of a detailed analysis on what is the appropriate percentile of the extreme aerodynamic pressure coefficient for tornadoes, the 78% percentile is used as the nominal maximum value, following the work by Cook and Mayne (1980). Roueche et al. (2020) used 50%.

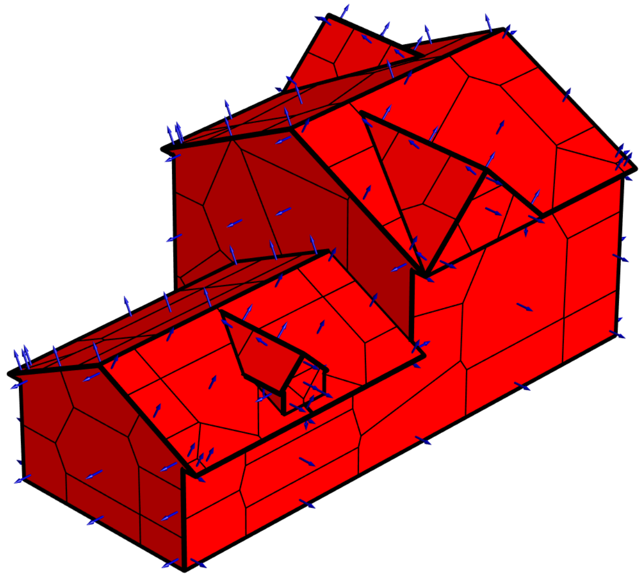

Fig 6. Tributary areas for each tap for House 2

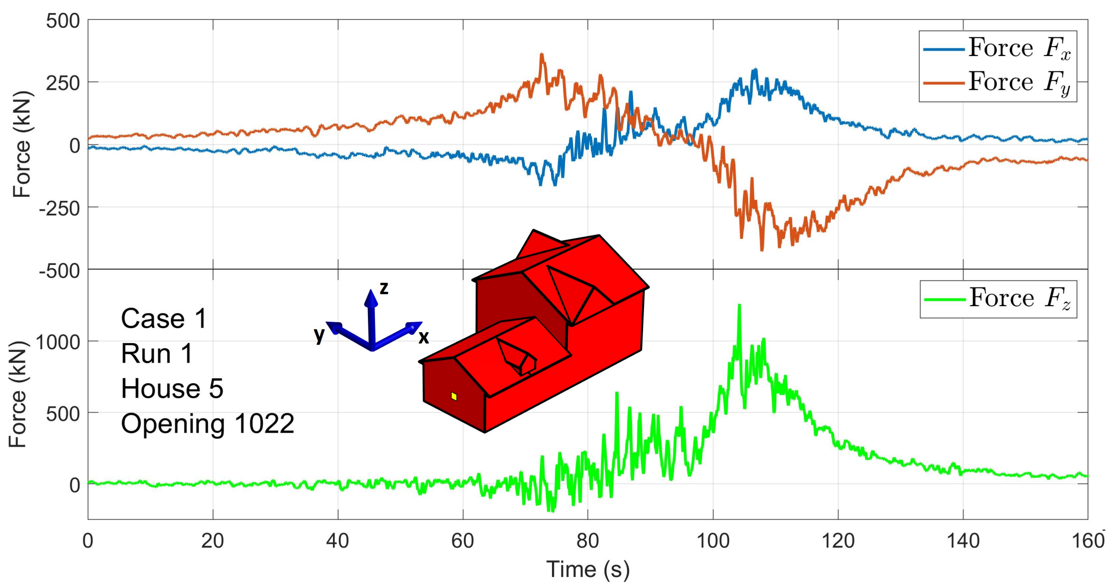

Fig 7. Overall force time histories in full-scale at House 5, in Case 1, Run 1 with internal pressure simulated for the opening scenario with the opening located on the yellow square.

3.4. Velocity scales

The full-scale pressures are calculated using dimensional analysis. Assuming equality of pressure coefficients at full-scale $\left(C_{p_{FS}}\right)$ and model scale $\left(C_{p_{MS}}\right)$ leads to

$$\frac{p_{MS} - p_{ref_{MS}}}{p_{FS} - p_{ref_{FS}}} = \lambda_V^2 \tag{8}$$

where p_{MS} and p_{FS} are the pressure at the same building location in model and full-scale respectively, $p_{ref_{MS}}$ and $p_{ref_{FS}}$ are the reference pressure in model and full-scale respectively, and the velocity scale is

$$\lambda_V = \frac{V_{ref_{MS}}}{V_{ref_{FS}}} \tag{9}$$

where $V_{ref_{MS}}$ and $V_{ref_{FS}}$ are reference velocities in model and full-scale respectively. Both reference velocity and pressure must be equivalent at model and full-scale. This means that, if for instance, $V_{ref_{FS}}$ is a 3-second gust, then $V_{ref_{MS}}$ must also be an equivalent 3-second gust (3-seconds at model scale). The term "3-second gust" refers to the expected value of the 3-second moving average peak of the wind speed in full-scale.

In the same way, assuming equality of force coefficients in full-scale ($C_{F_{FS}}$) and in model scale ($C_{F_{MS}}$) leads to

$$\frac{\mathbf{F}_{MS}}{\mathbf{F}_{FS}} = \lambda_V^2 \lambda_L^2 \tag{10}$$

where $\mathbf{F}_{MS}$ and $\mathbf{F}_{FS}$ are forces in model and full-scale respectively. λ_L is the length scale defined as the ratio of the model to full-scale reference lengths.

The length scale is readily available from the geometric scale used for the model, $\lambda_L = 1/150$. This geometric scale was selected as a compromise between the need for the buildings to be large enough to fit a considerable number of pressure taps and the TLVs length scale presented in Table 1. The model scale is slightly higher than the TLVs scale. The determination of the velocity scale is more complicated. As explained before, ASCE/SEI 7-16 and ASCE/SEI 7-22 use a 3-second gust design wind speed. ASCE/SEI 7-16 uses, as design wind speed, the end-of-range of the EF category of the tornado being considered which is a 3-second gust velocity, and ASCE/SEI 7-22 uses a 3-second gust velocity with a return period that depends on the Risk Category of the structure, its plan area, and its location.

The physically simulated TLVs are characterized by a maximum mean velocity, which is the maximum temporal average of the tangential velocity measured in a stationary condition. Since both reference velocities have different meanings (full-scale is a 3-second gust and model is a mean velocity), one of them must be transformed to find two equivalent reference velocities. For instance, the full-scale reference 3-second gust velocity has to be transformed to a mean velocity in full-scale or the model mean velocity has to be converted to an equivalent 3-second gust velocity at model scale.

The transformations between mean and 3-second gust velocity make use of a tornado velocity gust factor G_{vTor} defined as follows:

$$G_{vTor}\left(t,T\right)=E\left[\frac{\hat{u}\left(t,T\right)}{\overline{U}}\right] \tag{11}$$

where $\hat{u}\left(t,T\right)$ is the peak value of the moving average velocity with a window width t in the period T, $\overline{U}$ is the mean velocity for the period T, and $E\left[\cdot\right]$ denotes expected value.

In the past, researchers have used a variety of values and methods to determine the gust factors for tornadoes. Wang and Cao (2021) and Haan Jr et al. (2010) used the Durst curve, which was derived for ABL flows, to obtain a gust factor. Haan Jr et al. (2010) explained that the use of the Durst curve is not ideal, but at the time there were no turbulence measurements within tornadoes or TLVs available which could have allowed for a more accurate determination. The value used by Wang and Cao (2021), $G_{vTor}=1.57$, is the gust factor with a 1-second averaging window and $T=3600s$. The gust factor utilized by Haan Jr et al. (2010), $G_{vTor}\approx 1.4$, was determined for a 3-second averaging window and a period equivalent at full-scale to the averaging time selected, which translated to between 310s and 450s in full-scale.

Roueche et al. (2020) used a different approach. Their reference velocity in model scale was calculated as the average of the maximums of the 3-s equivalent moving average of the wind velocity time history measured using cobra probes. The 3-second equivalent window width was found using a fixed velocity scale.

In this research, we propose an iterative method for evaluating the velocity scale and velocity gust factor. More specifically, the wind speed measurements of the stationary TLVs are utilized in the following way:

1. A velocity gust factor G_{vTor} is assumed.
2. With the velocity gust factor, a velocity scale can be calculated using:

$$\lambda_V = \frac{V_M G_{vTor}}{V_{FS}} \tag{12}$$

   where V_M is the average maximum tangential wind speed (Table 1) and V_{FS} is the 3-second gust wind speed in the target tornado EF-rating, i.e. end-of-range speed for the EF rating being considered (Table 3).
3. A time scale is calculated as

$$\lambda_T = \frac{\lambda_L}{\lambda_V} \tag{13}$$

4. Find the 3-second equivalent window width (w_s) in samples by

$$w_s = 3 \cdot \lambda_T \cdot f \tag{14}$$

   where $f = 500Hz$ is the sampling frequency. The window size equivalent to w_s but in seconds is denoted by w_t.
5. Apply a moving average with window width w_s to the measured velocity time history (model).
6. Divide the obtained 3-second equivalent time history into an appropriate number of segments. Here, the time history is divided into 10 segments with 6016 samples each. The number of segments is arbitrary but has an influence on the value of the gust factor obtained, therefore, it must be selected carefully. The length of the segments, here, is representative of a medium-lived tornado. Fig. 8 illustrates this process graphically for EF3-rated TLV.
7. For each segment the maximum 3-second equivalent gust ($V_{3s,max,i}$) is found along with the average velocity ($V_{mean,i}$), where i denotes the i-th segment.
8. Calculate the velocity gust factor as the average of the quotient between the maximum 3-second velocity and the average velocity, for the 10 segments:

$$G_{vTor} = \frac{1}{10} \sum_{i=1}^{10} \frac{V_{3s,max,i}}{V_{mean,i}} \tag{15}$$

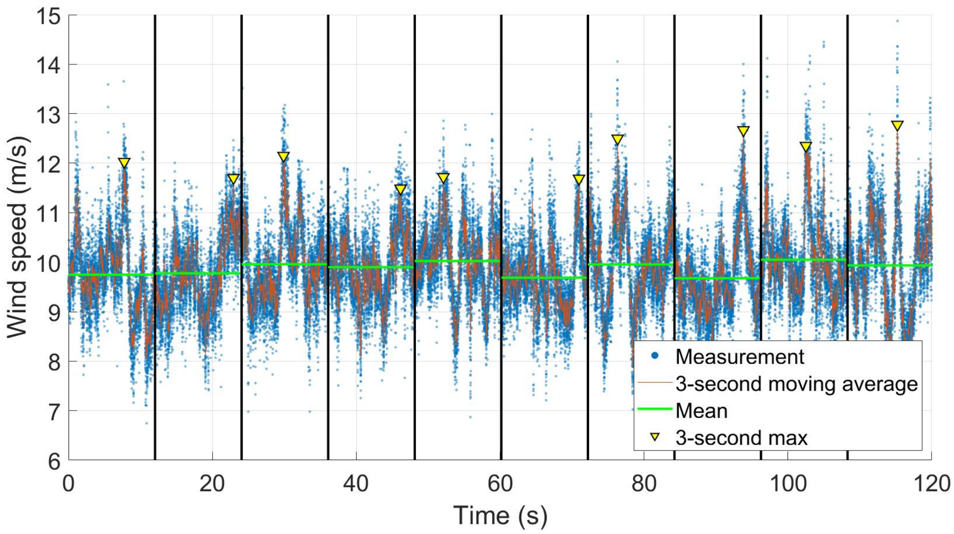

Fig 8. Wind velocity measurement at RMW for EF3-rated stationary TLV showing the maximum 3-second equivalent (in model time) gust and mean on each segment for the calculation of the velocity gust factor.

9. If the difference between the calculated velocity gust factor and the one assumed in Step 1 is higher than a specified tolerance, go back to Step 1 but using G_{vTor} obtained in Step 8 and repeat Steps 1 to 9. If the difference is less than the selected tolerance, stop the iteration.

This process converges in less than 10 iterations for a 0.001 tolerance and leads to the values presented in Table 4.

Table 4

Scales and parameters of the TLVs scaled to EF end-of-range tornadoes.

Rating	Segment length (s)	λ_V	λ_T	$w_t(s)$	$w_s(samples)$	$G_{vTor,ref}$
EF1	586	1:3.08	1:48.7	0.062	31	1.39
EF2	514	1:3.51	1:42.8	0.070	35	1.25
EF3	486	1:3.71	1:40.4	0.074	37	1.23

The values of the velocity gust factor decrease as the rating increases. This suggests the turbulence intensity decreases for higher tornado ratings which can be attributed to reduced wandering. See Ashton et al. (2019) for a description of TLVs wandering.

It is important to note the limitations of the method used. The velocity record was split into 10 segments that roughly corresponds to 10-minute duration tornadoes, this may not be appropriate for all tornado rating. In addition, here, the TLVs are scaled to EF end-of-range tornadoes which may be inappropriate, specifically when ASCE 7-22 prescribes a design wind speed that varies according to location, plan area, and type of structure.

The 3-second averaging window width is selected to match the velocity scale in the proposed method, in contrast to Roueche et al. (2020), where the window is fixed.

The value of the gust factor can influence the ratios between WindEEE obtained and code calculated loads r because

$$r \propto G_{vTor}^{-2}. \tag{16}$$

A high gust factor leads to low values of the ratio and vice versa.

Different gust factors lead to different velocity scales and therefore, the scaled internal volume of the building is affected (see discussion in Section 3.5). This effect can change the behavior of the internal pressure and the results. In any case, since the resonant effects are low, we assume its influence on the internal pressure behavior could be negligible. As a result, any ratio of forces or pressures reported here (r_{ref} for $G_{vTor,ref}$) can be converted to a ratio for different gust factor G_{vTor} using

$$r = r_{ref} \left(\frac{G_{vTor,ref}}{G_{vTor}} \right)^2. \tag{17}$$

In other words, this equation and the obtained r_ref can be used to evaluate r if a different velocity gust factor is preferred.

3.5. Internal pressure

The internal pressure $p_{int}(t)$ is considered to mimic three different scenarios:

1. Completely sealed building
2. Nominally sealed with leakage
3. One dominant opening

These scenarios are selected to account for the different situations that can arise in terms of internal pressure for a low-rise building, i.e. (1) a building that is unable to quickly adapt its internal pressure to the changing overall external pressure, (2) a building that changes rapidly its internal pressure to follow the changes in external pressure and (3) a building that has a dominant opening and therefore the internal pressure is dominated by the interaction of the flow and the opening.

The internal pressure for the completely sealed building case is modeled as equal to the pressure measured inside the main chamber far from the TLV.

For each house, a number between 9 and 13 opening locations representative of failed windows or doors are being considered in the single dominant opening scenario. All openings are located on walls. Fig. 9 shows the location of some of the openings considered in House 7.

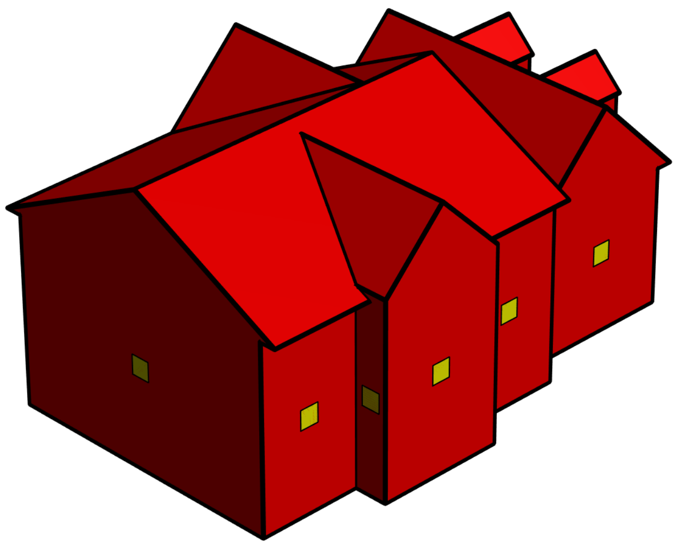

Fig 9. House 7 showing the location of some of the dominant openings considered.

For the nominally sealed and dominant opening case, the internal pressure on each house is modeled using the MDE (Oh et al., 2007):

$$
\begin{aligned}
\rho\ell_{e1}\ddot{x}_1 + \left(\frac{1}{k_1}\right)^{\frac{1}{n}} \left(\frac{\rho}{2}\right)^{\frac{1}{2n}} \dot{x}_1 \left|\dot{x}_1\right|^{\frac{1}{n}-1} &= p_{e,1} - p_{int} \\
\rho\ell_{e2}\ddot{x}_2 + \left(\frac{1}{k_2}\right)^{\frac{1}{n}} \left(\frac{\rho}{2}\right)^{\frac{1}{2n}} \dot{x}_2 \left|\dot{x}_2\right|^{\frac{1}{n}-1} &= p_{e,2} - p_{int} \\
&\vdots \\
\rho\ell_{em}\ddot{x}_m + \left(\frac{1}{k_m}\right)^{\frac{1}{n}} \left(\frac{\rho}{2}\right)^{\frac{1}{2n}} \dot{x}_m \left|\dot{x}_m\right|^{\frac{1}{n}-1} &= p_{e,m} - p_{int} \\
\sum_{j=1}^{m} \epsilon_j A_j \dot{x}_j &= \frac{V_{o,MS}}{\gamma p_o}\dot{p}_{int}
\end{aligned} \tag{18}
$$

where ρ is the density of air, ℓ_{ej} is the effective length, which represents the length of the "air slug" that goes in and out of the building, k_j is the discharge coefficient, n is the flow exponent which ranges from 0.5 if the flow through the leakage holes is laminar to 1 if is fully turbulent, $\dot{x}_j$ is the flow velocity through the opening assigned to tap j, and $\ddot{x}_j$ its acceleration, $p_{e,j}$ is the external pressure at tap j, P_{int} is the internal pressure, ϵ_j is the envelope porosity, A_j is the tributary area assigned to tap j, $V_{o,M}$ is the scaled volume of the model building, γ is the heat capacity ratio for air and p_o is the atmospheric pressure. Holmes (2007) proposes a value $\ell_e \approx 0.89\sqrt{A}$.

Since pressures are measured at model scale, the internal pressure is modeled at model scale also, which means the internal volume of the buildings must be properly scaled to account for resonant effects. The model scale internal volume $V_{o,M}$ can be calculated using (Oh et al., 2007):

$$
V_{o,M} = V_{o,FS}\frac{\lambda_L^3}{\lambda_V^2} \tag{19}
$$

where $V_{o,FS}$ is the full-scale internal volume of the building, λ_L is the length scale, and λ_V is the velocity scale.

In the distributed leakage case, we assume no significant opening is present in the building envelope, and therefore the passage of air in and out of the building is done through cracks in the envelope, utility ducts, and imperfect seal of the gaps between doors or windows and frames. In this way, the background leakage is assumed to be uniformly distributed on the walls of the building. The values of building envelope porosity ϵ, defined as the ratio of the total opening area to the total surface area of buildings, are highly scattered, ranging from 10^{-4} to 10^{-3} (Ginger, 2000). Here, we use a value of the porosity $\epsilon = 10^{-4}$, and the same value of the discharge coefficient used in Oh et al. (2007) for their distributed leakage case, $k = 0.38$. The exponent $n = 0.65$ is the value recommended by ASHRAE for full-scale buildings.

For the dominant opening scenario, the internal pressure is modeled with the same set of parameters as in the distributed leakage at all taps except the one where the opening is located. The result is one big opening with background leakage coupled. We assign the following values to the parameters at the opening: discharge coefficient $k = 0.63$, flow exponent $n = 0.65$, and opening area $A = 2.22 \cdot 10^{-5} m$ which corresponds to a $0.5m^2$ opening in full-scale.

The above differential equation system is solved numerically using an iterative backward differences scheme. The nonlinear algebraic system obtained after the discretization is solved using the Newton-Raphson method. A max tolerance between iterations of $Tol = 1 \cdot 10^{-8}$ was used as a stopping criterion.

An analysis of the optimum time step considering computation speed and solution accuracy was done. The solution to the MDE equations for one particular case, run and house, and case, run, house and opening was found using the Dormand-Prince adaptive Runge-Kutta method for the distributed leakage and opening cases respectively. The MATLAB® function ode45, which implements the Dormand-Prince method, was used for the calculation with absolute and relative tolerances 10^{-6} and 10^{-3} respectively.

This solution was assumed to be a good approximation of the exact solution. Then, the maximum error of the solutions of the faster iterative backward difference method was calculated by comparing to this "exact solution" for different time steps. Fig. 10 shows the absolute error in the internal pressure as a function of the time step for the distributed leakage and the opening case.

Time steps $Dt = 10^{-3}s$ and $Dt = 10^{-4}s$ for distributed leakage and opening scenarios were selected to keep the error lower than the uncertainty of the pressure measurements $\pm 0.3Pa$.

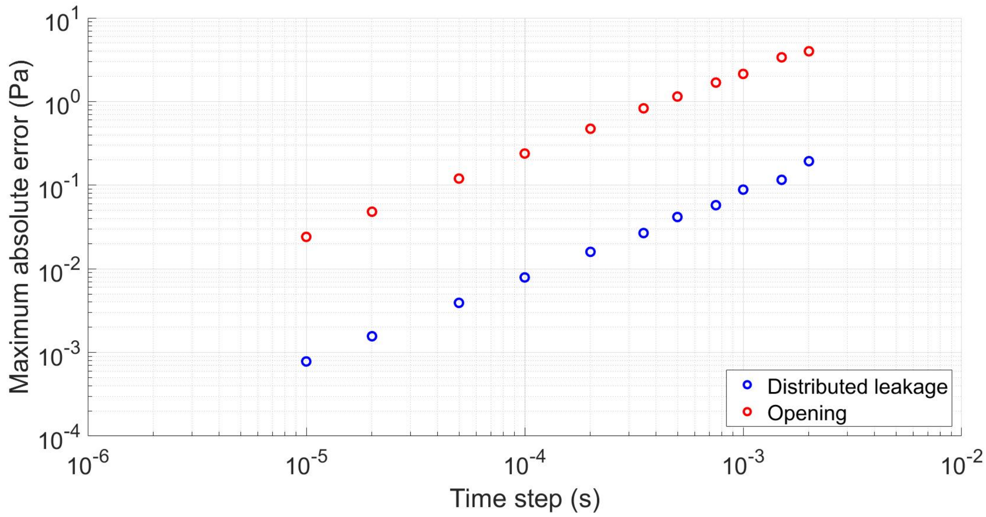

Fig 10. Maximum absolute error as a function of time step

Simulations for each case, run, and house for the distributed leakage scenario and case, run, house, and opening for the single opening scenario was performed. In total, 7560 opening simulations and 672 leakage simulations were completed.

4. Results

In this section, the ratios of the forces for MWFRS and pressures for C&C obtained from measurements and calculated using the standards are reported. The ratio of forces defined in the previous section r_{ref}, is calculated using

$$r_{ref} = \frac{F_{WindEEE}}{F_{ASCE}} \tag{20}$$

and the ratio of the pressures is calculated using

$$r_{ref} = \frac{p_{WindEEE}}{p_{ASCE}} \tag{21}$$

where the subscripts WindEEE and ASCE denote the method of calculation i.e. physical simulation measurements and ASCE/SEI 7-16 and 7-22 standard respectively. For the calculation of the ratios, the gust factors shown in Table 4 are used.

As was mentioned before, the force or pressure calculated from the WindEEE measurement represents the 78% percentile found using a Gumbel distribution fitted to the sample of maximums (runs) of the target variable.

The lateral forces F_x and F_y are the forces along the ridge of the house and transversal to the ridge respectively, while F_z is the vertical or uplift force (see Fig. 7). Only the uplift or upwards force is considered, the downwards force was ignored since it's not critical for wind loading. For pressures, only the net pressure acting in the outwards direction is considered. The net pressure is calculated as the difference between external and internal pressure.

ASCE/SEI 7-22 proposes three enclosure classifications relevant to this research i.e. Sealed, Enclosed, and Partially enclosed. Each classification leads to a different internal pressure value assignment as explained in Section 3. Note that since the internal pressure coefficient in both the Enclosed and Partially enclosed classifications is the same, only the Partially enclosed condition is analyzed.

The comparison offered here is performed between forces and pressures calculated using ASCE/SEI 7-16 extended method and ASCE/SEI 7-22 in the Sealed and Partially enclosed conditions on one hand and on the other hand the ones calculated from WindEEE Dome measurements under the three different internal pressure scenarios described in Section 3.5. The simulated internal pressure scenarios are "Distributed Leakage", "Opening", and "Sealed". There is a clear equivalence between the Sealed scenario and the Sealed classification in ASCE/SEI 7-22. The ASCE/SEI 7-22 Partially enclosed has its homologous in the Opening scenario. The Distributed leakage scenario has no counterpart in the standard but is included because it is representative of a building that retains the integrity of its envelope.

4.1. MWFRS

Fig. 11 shows the ratios of the force components on the whole house (see also Table A.1). Here, "DistLeak", "Opening" and "Sealed" denote "Distributed leakage", "Opening" and "Sealed" internal pressure scenarios, while "PartEnc" and "Sealed" denote Partially enclosed and Sealed enclosure classification.

The ratios presented in Fig. 11 are the maximum registered in any case or house with the same EF rating and force component. For example, the value of the ratio "DistLeak vs ASCE 7-16" for F_x and EF1 is registered at House 5 and Case 6 and for F_y and EF1 is found at House 7 and Case 6.

The ratios decrease as the tornado rating increases, which suggests that, as a general rule, a design to resist an EF3-rated tornado that is subjected to the design EF3-rated tornado

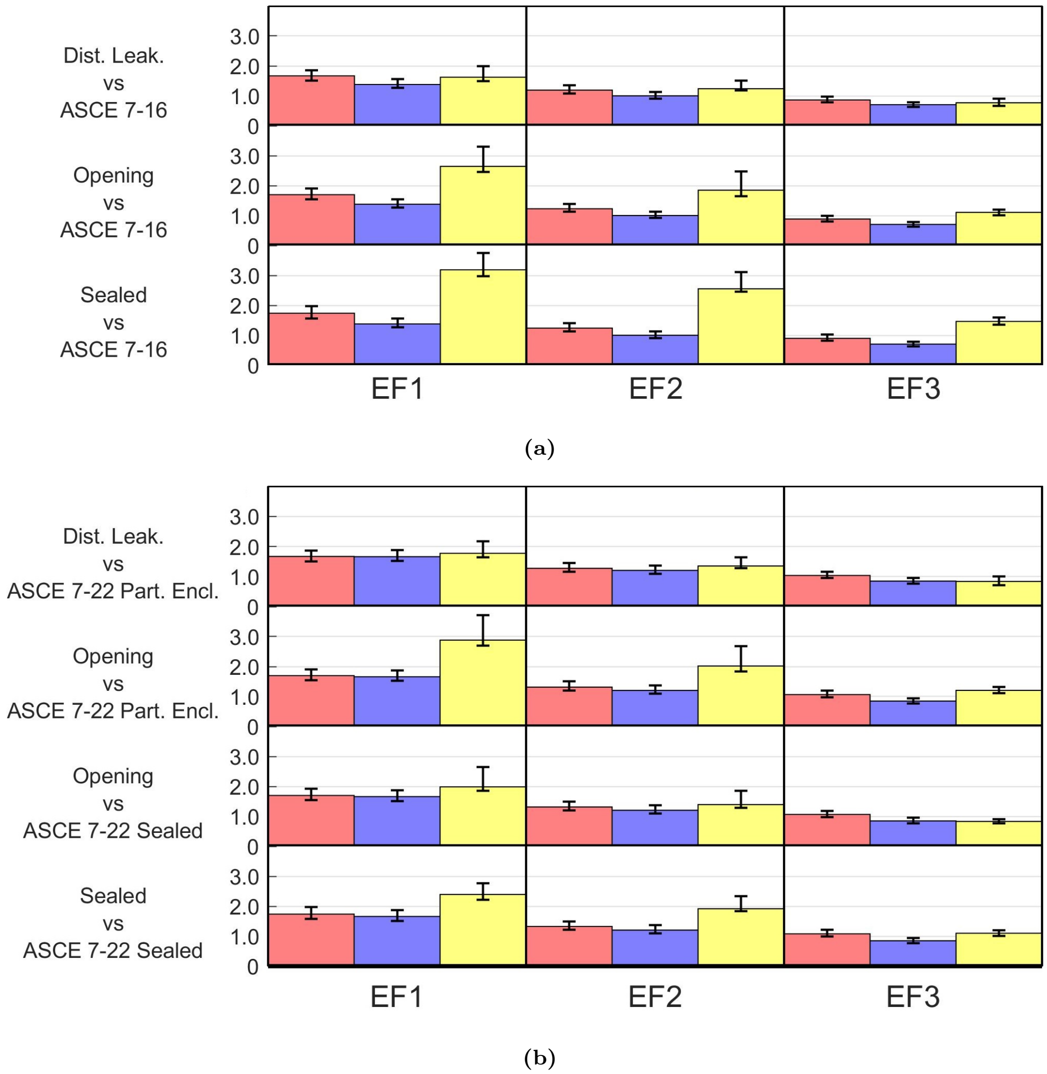

Fig 11. Ratios of overall forces for different comparisons and EF-ratings. Fx (red), Fy (blue), and Fz (yellow). (a) Comparison against ASCE/SEI 7-16, (b) comparison against ASCE/SEI 7-22. The whiskers indicate the 90% confidence intervals

would be safer than a design aimed to resist an EF2-rated tornado that is subjected to the design EF2-rated tornado and so on.

The ratios of lateral forces found for EF1-rated tornadoes are between 1.38 and 1.74, for EF2-rated tornadoes between 1.00 and 1.33, and for EF3-rated tornadoes between 0.70 and 1.08. The values are close together for the same EF rating and component, which can be explained by the fact that the internal pressure value does not influence the value of overall lateral forces. In most comparisons, the ratios for F_x are higher than the ratios for F_y, but similar.

The values of the uplift force ratios are all higher than 1.0, except for EF3-rated tornadoes. The lowest ratios for any EF rating, are found in both comparisons against the Distributed leakage scenario and "Opening vs ASCE7-22 Sealed". The highest values are found when comparing against the sealed scenario, followed closely by the Opening scenario. It is interesting to note that the ratios when comparing against the Opening scenario are close to the ones when comparing to the Sealed scenario. This means that an opening can create internal pressures of the same order of magnitude as the sealed condition.

In the event of a breach in the envelope, the uplift force can change dramatically reaching values of ratios as high as 2.64 and 2.88 for EF1-rated tornadoes in the relevant comparison between Opening and ASCE 7-16 and ASCE 7-22 Partially enclosed. These values decrease as the rating increase: 1.85 and 2.02 for EF2-rated tornadoes and 1.11 and 1.21 for EF3-rated tornadoes. This means an increase between 44% and 63% in the loads from the Distributed leakage scenario to the Opening scenario, which highlights the importance of keeping the integrity of the building's envelope. These results indicate that the entire roof can be compromised if breaches are created during the event of a tornado. This observation deserves to be taken carefully: for winds in the EF1 range, even though the ratios are high, the uplift forces may be too weak to overcome the roof's own weight and common roof-to-wall connections, on the other hand, for EF3-rated tornadoes, the ratios are lower, but the forces are higher, therefore a situation where the whole roof is lifted is more likely to occur. In addition, it is likely that other localized damages e.g. at the roof's corners occur before the entire roof can be lifted.

4.1.1. Comparison with previous studies

Fig. 12 presents the comparison of the maximum ratios of the base shear and uplift forces on the whole houses between measurements and code-based calculation reported by Wang and Cao (2021) and Haan Jr et al. (2010) and this research. In order to make a fair comparison, the analogous ratios to the ones calculated by the cited authors among the ratios calculated in this research are identified.

Wang and Cao (2021) compared the tornado-induced loads on a low-rise building obtained from wind tunnel simulations with the guidelines from ASCE/SEI 7-16. They measured the internal pressure and simulated four cases which represent two internal pressure scenarios i.e. distributed leakage and one dominant opening. The swirl ratio used in their research was 0.72 which corresponds to an EF3-rated tornado according to the authors. Accordingly, their results are compared in two ways: first, their distributed leakage vs ASCE/SEI 7-16 is compared to the Dist.Leak. vs ASCE/SEI 7-16 for EF3 tornadoes in this research and their one dominant opening vs ASCE/SEI 7-16 was compared to the Opening vs ASCE/SEI 7-16 for EF3-rated tornadoes in this research.

Haan Jr et al. (2010) calculated the ratios between the overall forces on a simple gable roof low-rise building and the provisions in ASCE 7-05. It is important to note that ASCE 7-05 didn't have provisions nor guidelines for tornado-resistant design, therefore, the authors adapted the parameters, originally intended for ABL flows, to fit tornadoes. In addition, they simulated several swirl ratios and reported the maximum base shear and uplift ratios. Also, they didn't consider internal pressure, consequently, their results are equivalent to the Sealed scenario in this research, therefore their ratios are compared to the Sealed vs ASCE 7-16.

4.2. Components & cladding (C & C)

Here, in Fig. 13 and Table A.2, the ratios of pressure in different zones and EF rating are presented. The zones are defined in Chapter 30 of ASCE/SEI 7-16, Figures 30.3-1, and 30.3-2C, and can be seen in Fig. 4. The maximum values of the pressure coefficients are utilized. These values correspond to the least EWA i.e. less than $0.2m^2$ for zone 3r and $0.9m^2$ for all other zones. Hence, the values of the external pressure coefficient C_p are the

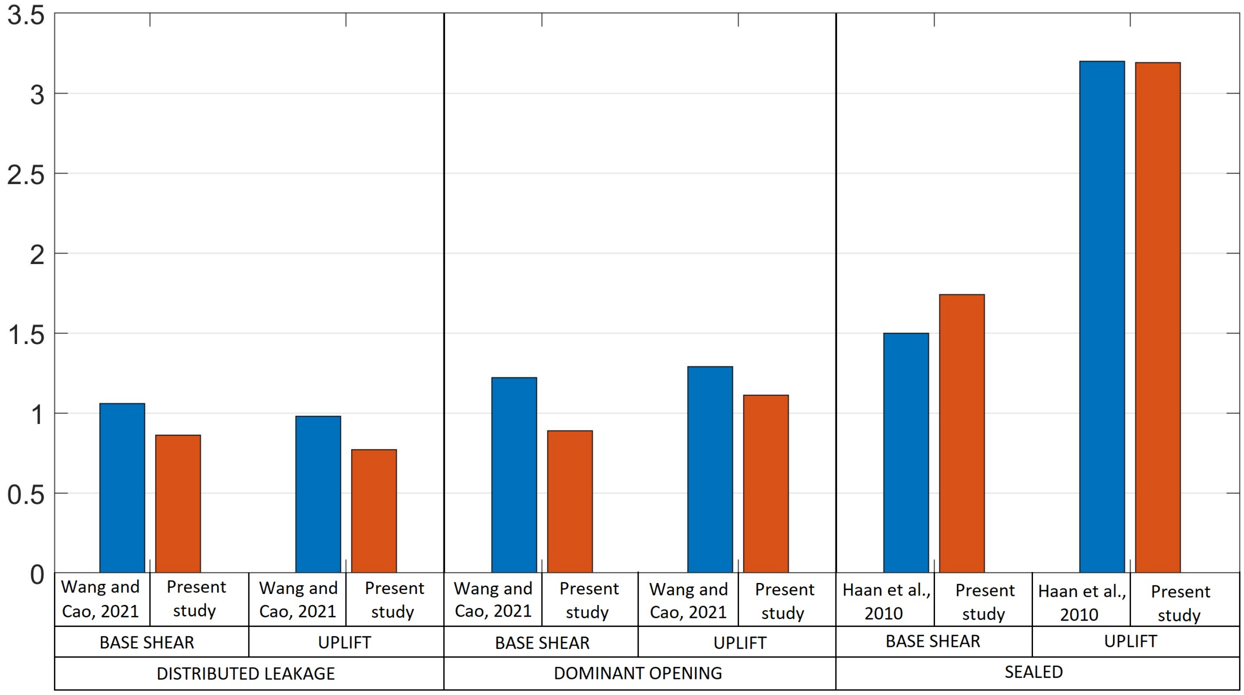

Fig 12. Comparison of the maximum ratios of the base shear and uplift force on the whole houses between measurements and code-based calculation reported by Wang and Cao (2021) and Haan Jr et al. (2010) and this research.

following: -1.5 for zones 1 and 2e, -2.5 for zones 2n, 2r and 3e, -3.0 for zone 3r, -1.1 for zone 4 and -1.4 for zone 5.

The two most relevant C&C comparisons reported in this article are: "Dist.Leak vs ASCE 7-22 Part.Enc. & Enc." and "Opening vs ASCE 7-22 Part.Enc. & Enc." because ASCE/SEI 7-22 is the current standard and the first to include a chapter for tornado loads and the "Opening" and "Distributed leakage" are the two most common enclosure scenarios that can arise in the event of a tornado.

In the case "Dist.Leak vs ASCE 7-22 Part.Enc. & Enc." most ratios are lower than 1.0. On the roof, only the ratios for EF1-rated tornadoes and zones 2e, and 3e are higher than 1.0 but close to one.

For the "Opening vs ASCE 7-22 Part.Enc. & Enc." comparison, the ratios on the roof zones for EF1-rated tornadoes are all higher than 1.0 except for zone 3r. The highest values are found for zones 2e and 3e with ratios of 1.77 and 1.83. For EF2-rated tornadoes, the value for zones 2e and 3e are higher than one with values 1.25 and 1.35 respectively. For EF3-rated tornadoes, only the ratio for zone 3e is higher than 1.0. The ratios are higher on the zones close to the eaves, i.e. zones 2e and 3e. This suggests the loading mechanism may be different than in ABL winds and that this mechanism is more pronounced in lower-rated tornadoes.

Almost all ratios on wall zones 4 and 5 are higher than 1.0. A maximum ratio of 2.48 is registered in the comparison "Sealed vs. ASCE 7-22 Part.Enc Enc.", for EF1-rated tornadoes in zone 5. In the "Opening vs. ASCE 7-22 Part.Enc. Enc." comparison, the ratios are between 1.99 and 2.02 for EF1-, between 1.69 and 1.97 for EF2-, and between 1.34 and 1.44 for EF3-rated tornadoes. This is consistent with the observation of sidewalls blowing outwards during tornado events when openings are present (Marshall, 2002).

It is important to note that the presence of openings increases the ratios on all zones (on walls and roof) between 9% and 56% with an average increase of around 32%, and a median of 28%, again, highlighting the importance of maintaining the integrity of the envelope.

The comparison Sealed against Sealed leads to similar values than "Opening vs ASCE 7-22 Part.Enc. & Enc." but there is an overall reduction of the values. The reduction comes from the higher internal pressure coefficient used.

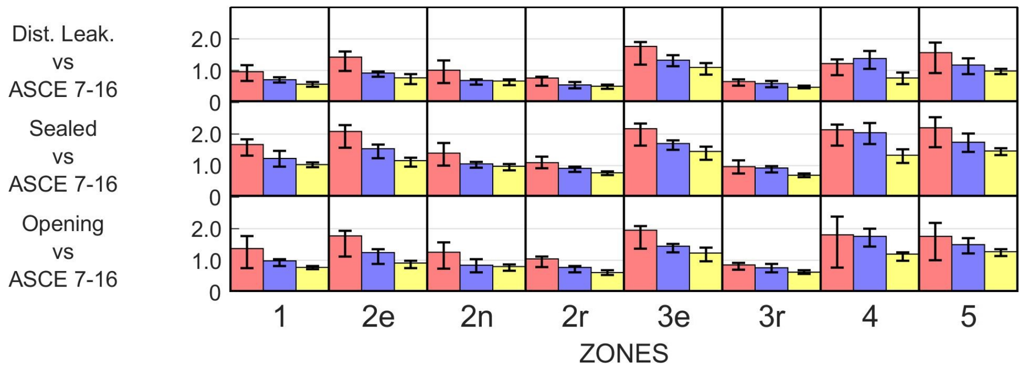

(a)

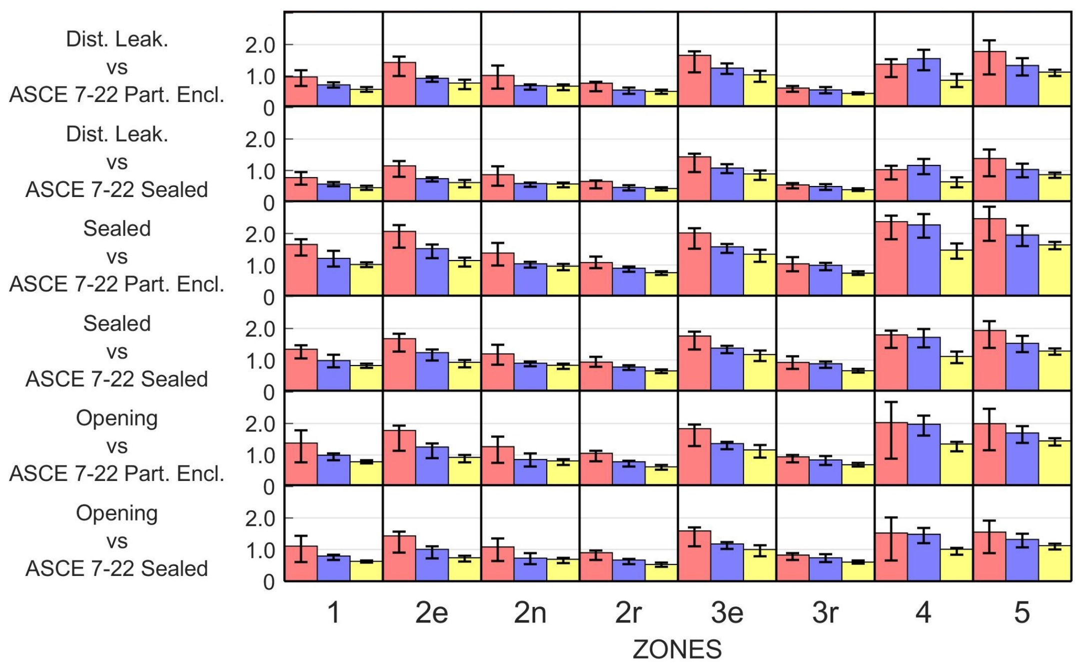

(b)

Fig 13. Ratios of pressures for different comparisons and zones. EF1 (red), EF2 (blue), and EF3 (yellow). (a) Comparison against ASCE/SEI 7-16, (b) comparison against ASCE/SEI 7-22. The whiskers indicate the 90% confidence intervals

4.3. Ratios uncertainty estimation

The most important sources of uncertainty in the reported ratios are: (1) the small sample size due to the number of runs available for each case i.e. between 5 and 10 runs, (2) the value of the velocity gust factor, (3) measurement uncertainties, and (4) the statistical model adopted to describe the distribution of the maximums, i.e. Gumbel distribution.

The limited sample size arises from the cost and time constraints imposed by this type of physical simulation at the WindEEE Dome. The number of samples necessary to eliminate the small sample size effect is unknown. For comparison, Haan Jr et al. (2010) and Case et al. (2014) used 10 runs and Roueche et al. (2020) 5 runs.

The determination of the minimum sample size for Generalized Extreme Value Distribution (GEVD) quantile estimation was studied by Cai and Hames (2010). They developed a method that uses the Shapiro-Wilk normality test on the bootstrapped maximum likelihood estimators (MLE) of the distribution parameters for a prescribed significance level (α). The number of samples must be increased until the $p-value > \alpha$, which would indicate that the null hypothesis (normality) can't be rejected. With this criterion, for $\alpha = 0.05$, both 5 and 10 runs are insufficient to describe adequately the population of maximums.

As was mentioned before, the value of the velocity gust factor adopted, can have a significant influence on the ratios. Since the gust factors are calculated as the average of the ratios between peak and mean in segments of the velocity time history measured in stationary TLVs, if the underlying distribution is normal, the gust factor has a Student-t distribution with $n - 1 = 10 - 1 = 9$ degrees of freedom, and $\sigma = S/\sqrt{n}$ and $\mu = \overline{x}$, where S^2 and $\overline{x}$ are the sample variance and mean respectively. The assumption that the underlying distribution is normal is reasonable as can be observed from the normal probability plots in Fig. 14. Fig. 15 shows normalized histograms of the bootstrapped velocity gust factors along with the Student-t and normal distribution with σ and μ calculated as explained before, showing good agreement.

Measurement uncertainties are judged to be of a lower order than the uncertainties generated by the low number of runs and the velocity gust factor, and therefore are not evaluated.

It is assumed that the maximums have Type I Extreme Value Distribution or Gumbel distribution. The epistemic uncertainty associated with this assumption can be reduced if

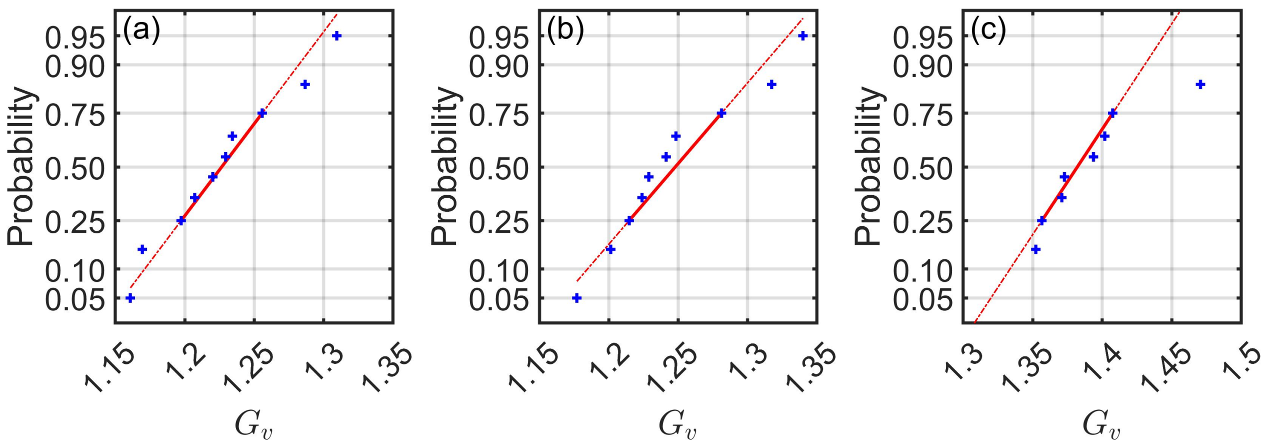

Fig 14. Normal probability plots of the ratios between peak and mean in the 10 segments. (a) EF1, (b) EF2, and (c) EF3.

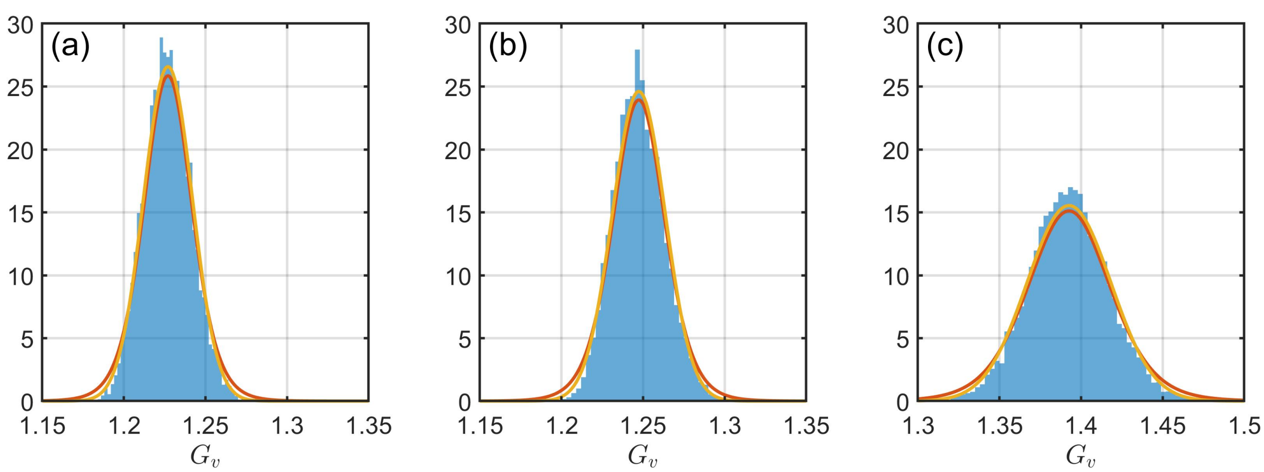

Fig 15. Normalized histograms of the bootstrapped ratios between peak and mean velocities, and Student-t (red) and Normal (yellow) distribution fitted.

additional samples are available, which is beyond the scope of this research.

The uncertainty in the ratios is estimated using the parametric bootstrap method (Davison and Hinkley, 1997). The steps of the procedure are:

1. From the list of maxima i.e. the maximums on each repetition (run), a high number (10000) of resamples (with replacement) are found.
2. For each resample, a set of parameters of the Gumbel distribution are obtained by fitting them using Lieblein's BLUE method.
3. With each set of parameters, the nominal peak (78% percentile) is obtained.
4. From a Student-t distribution with σ and μ calculated as explained before, values of the velocity gust factor are randomly generated (10000).
5. A set of 10000 ratios is calculated using the nominal peaks and velocity gust factors.
6. The two-sided 90% confidence interval is found from the 5% and 95% percentiles. These limits are used to report uncertainties in the ratios in Fig. 11 and Fig. 13 and Table A.1 and Table A.2.

Fig. 16 shows the normalized histograms of the 78% percentile of the ratio in Case 1, House 5, Zone 3r, and Tap 1319 with 9 runs (blue) and 5 runs (red). This highlights the reduction of the uncertainty in the ratios by increasing the number of runs.

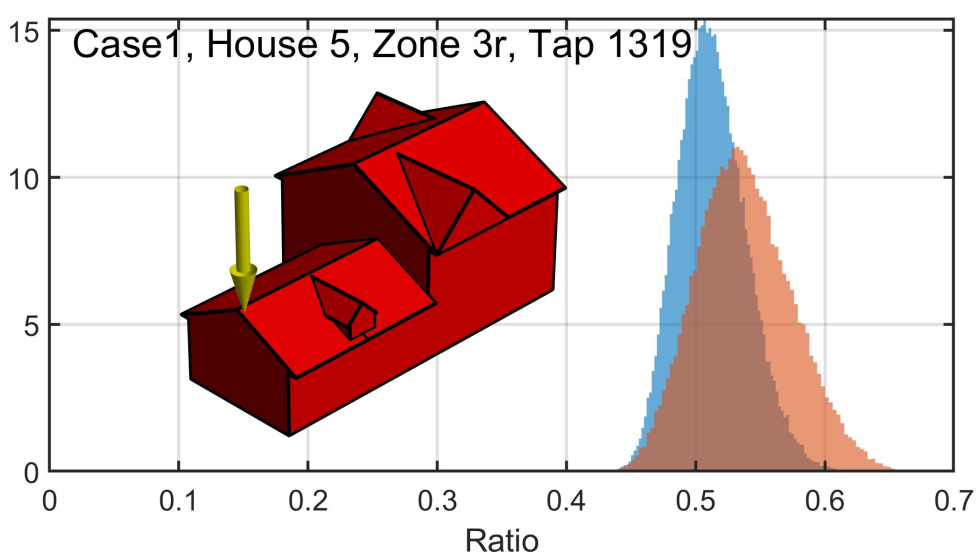

Fig 16. Normalized histograms of the ratios for 9 runs and 5 runs.

If the samples are not representative of the population, which can happen when the number of samples (runs) is low, it is possible for the calculated variability of the ratios to be mistakenly less with fewer samples than with more samples.

4.4. Discussion

As was mentioned in Section 3, the pressure coefficients for C&C are found in Figures 30.3-1 and 30.3-2C in ASCE/SEI 7-16 and 7-22, for an EWA of 0.19 ft^2. For low EWAs the pressure coefficients are independent of the value of the EWA in the standards. This is mostly because there is a lack of pressure-averaged data for low EWAs, not because the pressure coefficients are actually independent of the EWA. In addition, very low EWAs are deemed not relevant since most components have EWAs of at least 10 ft^2.

Since in this research, the measured pressure is a point pressure (EWA=0.19 ft^2), it may result in an unfair comparison because the pressure coefficients from the standards are actually area averages with larger EWA $\approx 10 ft^2$.

The decision was made here to use the values from the standards as they come (C_{pref}), but other criteria may be valid, for instance, as suggested in Appendix C30 of ASCE/SEI 7-22, a practitioner may choose to extrapolate the sloped part of the EWA-C_p plots in Figures 30.3-1 and 30.3-2C to smaller EWAs, as shown in Fig. 17a, Fig. 17b and Fig. 17c. This leads to higher absolute value pressure coefficients which are much more conservative.

The reported ratios r_{ref} can be converted for different C_p with

$$r = r_{ref} \cdot \frac{0.9GC_p - 0.55}{0.9GC_{p_{ref}} - 0.55} \tag{22}$$

for ASCE/SEI 7-16 and

$$r = r_{ref} \cdot \frac{0.75K_{vT}GC_p - GC_{pi}}{0.75K_{vT}GC_{p_{ref}} - GC_{pi}} \tag{23}$$

for ASCE/SEI 7-22, where the values of $C_{p_{ref}}$ and K_{vT} are presented in Table 5. GC_{pi} is +0.55 for Enclosed or Partially enclosed classifications and +1.0 for the Sealed classification.

5. Conclusions

The goal of this study was to compare the design tornado-induced loads provided by ASCE/SEI 7-22 and ASCE/SEI 7-16 against what would be experienced by real-world shaped

Table 5

Reference pressure coefficients for ASCE/SEI 7-16 and 7-22, and the external pressure coefficient adjustment factor for vertical winds used for each zone in ASCE/SEI 7-16, with the corresponding zone in ASCE/SEI 7-22 in parenthesis.

	Zone							
	1 (1)	2e (1)	2n (2)	2r (2)	3e (2)	3r (3)	4 (4)	5 (6)
$C_{p_{ref}}$ ASCE 7-16	-1.5	-1.5	-2.5	-2.5	-2.5	-3.6	-1.1	-1.4
$C_{p_{ref}}$ ASCE 7-22	-1.5	-1.5	-2.5	-2.5	-2.5	-3.0	-1.1	-1.4
K_{vT}	1.2	1.2	1.2	1.2	1.2	1.3	1.0	1.0

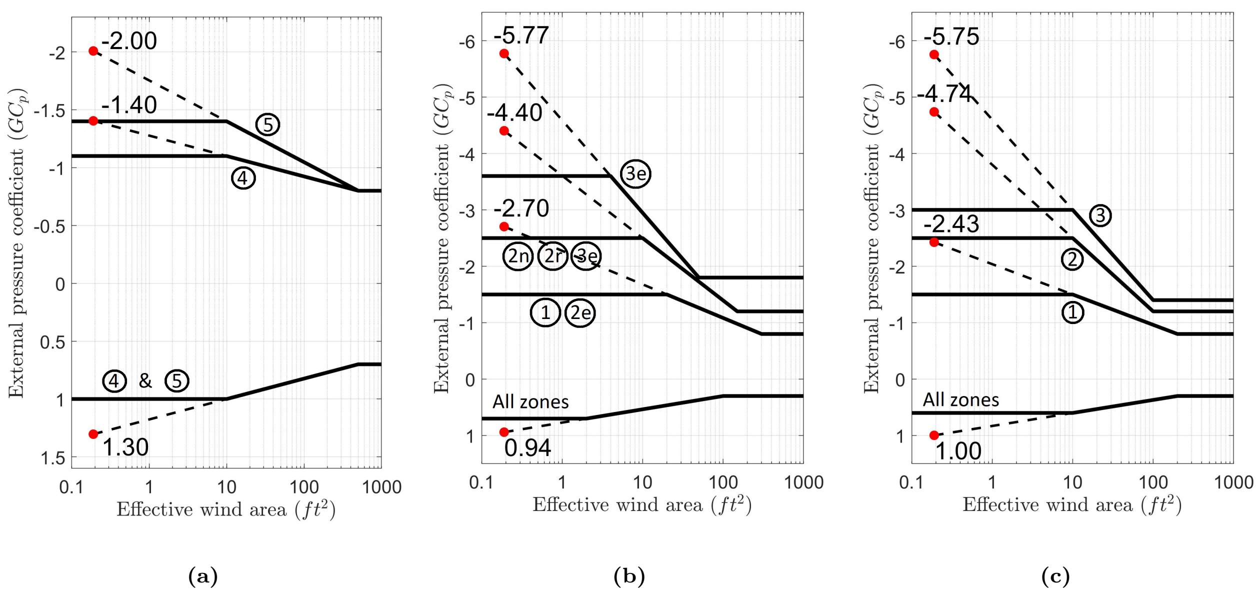

Fig 17. External pressure coefficients as a function of EWA. (a) On the walls for both ASCE/SEI 7-16 and 7-22, (b) on the roof for ASCE/SEI 7-16, and (c) on the roof for ASCE/SEI 7-22 (reproduced from ASCE (2017) and ASCE (2022))

low-rise residential buildings forming a community during tornado events of different intensities.

Physical simulation in the WindEEE Dome at UWO was employed to investigate this issue. Pressures and forces on 8 model houses in a community were measured while interacting with several translating TLVs with different characteristics, representative of EF1-, EF2- and EF3-rated tornadoes, with a diversity of paths and trajectories. Three internal pressure scenarios were simulated numerically using the MDE model.

The tornado velocity gust factor was identified as a critical parameter when translating loads from model scale to full-scale. A method using stationary TLVs velocity measurements at RMW was developed for its calculation. The values of the tornado velocity gust factor decrease as the tornado rating increases which can be attributed to the increased wandering effect at lower ratings.

The comparison of the loads suggests that, in general, a structure designed to resist a certain EF-rated tornado subjected to the same considered EF-rated tornado would be safer as the rating increases, more specifically, if for instance, a building is designed to withstand an EF3-rated tornado using ASCE/SEI 7 standards, it would be safer than if it is designed to resist an EF2-rated tornado in the case the design tornado actually hits the structure, and so on.

The ratios of overall uplift forces increase between 44% to 63% from the distributed leakage scenario to the one dominant opening scenario. This implies that in case of breaches in the envelope, the increase in uplift force can be significant, highlighting the need to keep the integrity of the envelope. Similar increments are observed in roof pressures.

A reasonable agreement was found when comparing the maximum overall load ratios reported by previous studies and this research.

It appears that pressures on walls are underestimated by the standards in most internal pressure scenarios and tornado ratings.

On the roof, the ratios are predominantly lower than 1.0, with few exceptions. Ratios for EF1-rated tornadoes are mostly higher than 1.0, and the values in zones 2e and 3e are often higher than one. The fact that ratios close to the eaves are higher than ratios on central parts of the roof and close to the ridge suggests that there is a different mechanism generating the peak pressures which is intensified in lower-rating tornadoes.

Declaration of competing interest

The authors declare that they have no known competing financial interests or personal relationships that could have appeared to influence the work reported in this paper.

Acknowledgments

The first author acknowledges partial support from Agencia Nacional de Investigación e Innovación (ANII) and CALDO. This work was supported by Mitacs through the Mitacs Accelerate program. The authors would like to thank Gerald Dafoe and Tristan Cormier for preparing and conducting the experiments. We also thank Daniel Davalos for his help in drawing the CAD model of the community.

Appendix A. Tables of force and pressure ratios.

Table A.1

Ratios of the overall force components calculated from the WindEEE Dome measurements to the calculations performed according to the standards. In parenthesis the 90% confidence intervals and in bold the ratios that are higher than 1.0

	EF1			EF2			EF3		
	Fx	Fy	Fz	Fx	Fy	Fz	Fx	Fy	Fz
DistLeak vs ASCE716	**1.67** (**1.47**,**1.83**)	**1.38** (**1.20**,**1.49**)	**1.62** (**1.25**,**1.75**)	**1.19** (**1.03**,**1.30**)	**1.00** (0.87,**1.09**)	**1.24** (0.98,**1.30**)	0.86 (0.75,0.93)	0.70 (0.62,0.77)	0.77 (0.63,0.88)
Opening vs ASCE716	**1.70** (**1.49**,**1.86**)	**1.38** (**1.21**,**1.49**)	**2.64** (**1.98**,**2.83**)	**1.23** (**1.07**,**1.34**)	**1.00** (0.87,**1.09**)	**1.85** (**1.22**,**2.04**)	0.89 (0.78,0.96)	0.70 (0.62,0.78)	**1.11** (**1.01**,**1.20**)
Sealed vs ASCE716	**1.74** (**1.51**,**1.92**)	**1.38** (**1.19**,**1.49**)	**3.19** (**2.63**,**3.40**)	**1.24** (**1.08**,**1.35**)	**1.00** (0.87,**1.10**)	**2.55** (**2.00**,**2.65**)	0.90 (0.77,0.97)	0.70 (0.62,0.78)	**1.46** (**1.33**,**1.58**)
DistLeak vs ASCE722_PartEnc	**1.67** (**1.47**,**1.83**)	**1.66** (**1.44**,**1.80**)	**1.77** (**1.37**,**1.91**)	**1.27** (**1.09**,**1.39**)	**1.20** (**1.05**,**1.31**)	**1.35** (**1.06**,**1.42**)	**1.04** (0.91,**1.13**)	0.85 (0.75,0.93)	0.84 (0.68,0.96)
Opening vs ASCE722_PartEnc	**1.70** (**1.50**,**1.85**)	**1.66** (**1.44**,**1.79**)	**2.88** (**2.04**,**3.07**)	**1.31** (**1.12**,**1.42**)	**1.20** (**1.04**,**1.31**)	**2.02** (**1.36**,**2.19**)	**1.06** (0.93,**1.15**)	0.85 (0.75,0.93)	**1.21** (**1.10**,**1.30**)
Opening vs ASCE722_Sealed	**1.70** (**1.48**,**1.85**)	**1.66** (**1.44**,**1.81**)	**1.98** (**1.32**,**2.12**)	**1.31** (**1.13**,**1.42**)	**1.20** (**1.04**,**1.31**)	**1.39** (0.93,**1.51**)	**1.06** (0.94,**1.16**)	0.85 (0.75,0.93)	0.83 (0.75,0.89)
Sealed vs ASCE722_Sealed	**1.74** (**1.51**,**1.90**)	**1.66** (**1.45**,**1.80**)	**2.39** (**2.01**,**2.58**)	**1.33** (**1.16**,**1.44**)	**1.20** (**1.04**,**1.32**)	**1.92** (**1.51**,**2.01**)	**1.08** (0.94,**1.17**)	0.85 (0.75,0.93)	**1.10** (1.00,**1.18**)

Table A.2

Ratios of the pressures in C&C zones calculated from the WindEEE Dome measurements to the calculations performed according to the standards. In parenthesis the 90% confidence intervals and in bold the ratios that are higher than 1.0

		Zones							
	Rating	1	2e	2n	2r	3e	3r	4	5
Dist.Leak.	EF1	0.96 (0.68,**1.17**)	**1.42** (0.99,**1.60**)	**1.01** (0.60,**1.32**)	0.76 (0.52,0.81)	**1.76** (**1.18**,**1.89**)	0.65 (0.53,0.72)	**1.22** (0.86,**1.36**)	**1.56** (0.92,**1.88**)
vs	EF2	0.71 (0.63,0.79)	0.92 (0.80,0.98)	0.69 (0.56,0.73)	0.55 (0.43,0.63)	**1.33** (**1.13**,**1.48**)	0.59 (0.47,0.68)	**1.38** (**1.05**,**1.62**)	**1.17** (0.89,**1.38**)
ASCE 7-16	EF3	0.57 (0.49,0.64)	0.77 (0.58,0.88)	0.67 (0.54,0.73)	0.50 (0.43,0.55)	**1.10** (0.87,**1.23**)	0.47 (0.43,0.52)	0.77 (0.57,0.94)	0.99 (0.88,**1.05**)
Sealed	EF1	**1.66** (**1.31**,**1.82**)	**2.07** (**1.57**,**2.27**)	**1.39** (0.99,**1.72**)	**1.09** (0.91,**1.28**)	**2.16** (**1.63**,**2.33**)	0.96 (0.74,**1.15**)	**2.13** (**1.63**,**2.29**)	**2.19** (**1.57**,**2.53**)
vs	EF2	**1.22** (0.96,**1.45**)	**1.53** (**1.22**,**1.66**)	**1.05** (0.93,**1.11**)	0.91 (0.80,0.96)	**1.69** (**1.49**,**1.79**)	0.92 (0.78,0.98)	**2.04** (**1.67**,**2.35**)	**1.73** (**1.42**,**2.00**)
ASCE 7-16	EF3	**1.02** (0.94,**1.10**)	**1.15** (0.96,**1.24**)	0.97 (0.84,**1.04**)	0.76 (0.69,0.81)	**1.44** (**1.18**,**1.60**)	0.69 (0.63,0.75)	**1.32** (**1.08**,**1.50**)	**1.45** (**1.33**,**1.54**)
Opening	EF1	**1.37** (0.76,**1.77**)	**1.77** (**1.12**,**1.93**)	**1.26** (0.74,**1.57**)	**1.04** (0.79,**1.12**)	**1.95** (**1.36**,**2.08**)	0.86 (0.70,0.92)	**1.80** (0.77,**2.38**)	**1.76** (**1.01**,**2.18**)
vs	EF2	0.98 (0.82,**1.04**)	**1.25** (0.89,**1.36**)	0.85 (0.63,**1.03**)	0.78 (0.62,0.82)	**1.44** (**1.26**,**1.51**)	0.77 (0.62,0.88)	**1.76** (**1.43**,**1.99**)	**1.49** (**1.21**,**1.69**)
ASCE 7-16	EF3	0.78 (0.72,0.82)	0.92 (0.76,0.99)	0.80 (0.67,0.86)	0.61 (0.53,0.68)	**1.23** (0.98,**1.40**)	0.63 (0.57,0.68)	**1.20** (0.98,**1.25**)	**1.27** (**1.14**,**1.35**)
Dist. Leak.	EF1	0.96 (0.68,**1.17**)	**1.42** (0.99,**1.60**)	**1.01** (0.60,**1.32**)	0.76 (0.52,0.81)	**1.65** (**1.10**,**1.77**)	0.61 (0.49,0.67)	**1.37** (0.96,**1.52**)	**1.77** (**1.04**,**2.13**)
vs	EF2	0.71 (0.63,0.79)	0.92 (0.80,0.98)	0.69 (0.56,0.73)	0.55 (0.43,0.63)	**1.24** (**1.06**,**1.39**)	0.55 (0.44,0.63)	**1.54** (**1.18**,**1.82**)	**1.33** (**1.01**,**1.56**)
ASCE 7-22 Part.Enc. & Enc.	EF3	0.57 (0.49,0.64)	0.77 (0.58,0.88)	0.67 (0.54,0.73)	0.50 (0.43,0.55)	**1.03** (0.82,**1.15**)	0.44 (0.40,0.48)	0.86 (0.63,**1.05**)	**1.11** (0.99,**1.19**)
Dist. Leak.	EF1	0.78 (0.55,0.95)	**1.15** (0.80,**1.29**)	0.87 (0.52,**1.14**)	0.66 (0.44,0.70)	**1.43** (0.96,**1.54**)	0.55 (0.44,0.61)	**1.03** (0.73,**1.15**)	**1.38** (0.81,**1.66**)
vs	EF2	0.57 (0.51,0.64)	0.74 (0.65,0.79)	0.59 (0.48,0.63)	0.47 (0.37,0.54)	**1.08** (0.92,**1.21**)	0.50 (0.40,0.57)	**1.16** (0.89,**1.37**)	**1.04** (0.79,**1.22**)
ASCE 7-22 Sealed	EF3	0.46 (0.39,0.52)	0.62 (0.47,0.71)	0.58 (0.47,0.63)	0.43 (0.37,0.48)	0.89 (0.71,**1.00**)	0.40 (0.36,0.43)	0.65 (0.48,0.79)	0.87 (0.78,0.93)
Sealed	EF1	**1.66** (**1.31**,**1.82**)	**2.07** (**1.57**,**2.27**)	**1.39** (0.99,**1.72**)	**1.09** (0.91,**1.28**)	**2.03** (**1.53**,**2.18**)	**1.05** (0.81,**1.26**)	**2.38** (**1.83**,**2.57**)	**2.48** (**1.78**,**2.86**)
vs	EF2	**1.22** (0.96,**1.45**)	**1.53** (**1.22**,**1.66**)	**1.05** (0.93,**1.11**)	0.91 (0.80,0.96)	**1.59** (**1.40**,**1.67**)	1.00 (0.85,**1.07**)	**2.28** (**1.87**,**2.63**)	**1.96** (**1.61**,**2.26**)
ASCE 7-22 Part.Enc. & Enc.	EF3	**1.02** (0.94,**1.10**)	**1.15** (0.96,**1.24**)	0.97 (0.84,**1.04**)	0.76 (0.69,0.81)	**1.35** (**1.11**,**1.50**)	0.75 (0.69,0.81)	**1.48** (**1.21**,**1.68**)	**1.65** (**1.50**,**1.74**)
Sealed	EF1	**1.34** (**1.06**,**1.47**)	**1.68** (**1.27**,**1.83**)	**1.20** (0.85,**1.48**)	0.94 (0.79,**1.10**)	**1.76** (**1.33**,**1.90**)	0.93 (0.72,**1.11**)	**1.80** (**1.38**,**1.93**)	**1.93** (**1.39**,**2.24**)
vs	EF2	0.98 (0.77,**1.17**)	**1.23** (0.99,**1.34**)	0.90 (0.80,0.95)	0.78 (0.68,0.83)	**1.38** (**1.21**,**1.45**)	0.88 (0.75,0.95)	**1.72** (**1.41**,**1.98**)	**1.53** (**1.26**,**1.77**)
ASCE 7-22 Sealed	EF3	0.83 (0.76,0.89)	0.93 (0.78,**1.01**)	0.84 (0.72,0.89)	0.66 (0.59,0.70)	**1.17** (0.96,**1.30**)	0.66 (0.61,0.72)	**1.11** (0.91,**1.27**)	**1.28** (**1.17**,**1.36**)
Opening	EF1	**1.37** (0.76,**1.77**)	**1.77** (**1.12**,**1.93**)	**1.26** (0.74,**1.57**)	**1.04** (0.79,**1.12**)	**1.83** (**1.27**,**1.95**)	0.93 (0.76,1.00)	**2.02** (0.87,**2.67**)	**1.99** (**1.14**,**2.46**)
vs	EF2	0.98 (0.82,**1.04**)	**1.25** (0.89,**1.36**)	0.85 (0.63,**1.03**)	0.78 (0.62,0.82)	**1.35** (**1.18**,**1.42**)	0.84 (0.68,0.96)	**1.97** (**1.60**,**2.23**)	**1.69** (**1.37**,**1.92**)
ASCE 7-22 Part.Enc. & Enc.	EF3	0.78 (0.72,0.82)	0.92 (0.76,0.99)	0.80 (0.67,0.86)	0.61 (0.53,0.68)	**1.15** (0.91,**1.31**)	0.68 (0.62,0.74)	**1.34** (**1.10**,**1.40**)	**1.44** (**1.29**,**1.53**)
Opening	EF1	**1.11** (0.61,**1.43**)	**1.43** (0.91,**1.56**)	**1.08** (0.64,**1.35**)	0.90 (0.68,0.97)	**1.59** (**1.11**,**1.70**)	0.83 (0.67,0.89)	**1.52** (0.65,**2.01**)	**1.55** (0.89,**1.92**)
vs	EF2	0.80 (0.67,0.84)	**1.01** (0.72,**1.10**)	0.73 (0.54,0.89)	0.67 (0.54,0.70)	**1.18** (**1.02**,**1.23**)	0.74 (0.60,0.85)	**1.48** (**1.21**,**1.68**)	**1.32** (**1.07**,**1.50**)
ASCE 7-22 Sealed	EF3	0.63 (0.58,0.66)	0.74 (0.62,0.80)	0.69 (0.58,0.74)	0.53 (0.46,0.59)	**1.00** (0.79,**1.14**)	0.60 (0.55,0.66)	**1.01** (0.83,**1.06**)	**1.12** (**1.01**,**1.19**)

References

ASCE, 2017. Minimum design loads and associated criteria for buildings and other structures, American Society of Civil Engineers.

ASCE, 2022. Minimum design loads and associated criteria for buildings and other structures, American Society of Civil Engineers.

Ashrafi, A., Romanic, D., Kassab, A., Hangan, H., Ezami, N., 2021. Experimental investigation of large-scale tornado-like vortices. Journal of Wind Engineering and Industrial Aerodynamics 208, 104449.

Ashton, R., Refan, M., Iungo, G.V., Hangan, H., 2019. Wandering corrections from piv measurements of tornado-like vortices. Journal of Wind Engineering and Industrial Aerodynamics 189, 163–172.

Bienkiewicz, B., Dudhia, P., 1993. Physical modeling of tornado-like vortex and tornado effects on building loading, in: Seventh US Conf. on Wind Engineering, UCLA, CA, June, pp. 27–30.

Burrough, P.A., McDonnell, R.A., Lloyd, C.D., 2015. Principles of geographical information systems. Oxford university press.

Cai, Y., Hames, D., 2010. Minimum sample size determination for generalized extreme value distribution. Communications in Statistics—Simulation and Computation® 40, 87–98.

Case, J., Sarkar, P., Sritharan, S., 2014. Effect of low-rise building geometry on tornado-induced loads. Journal of Wind Engineering and Industrial Aerodynamics 133, 124–134.

Church, C., Snow, J., Baker, G., Agee, E., 1979. Characteristics of tornado-like vortices as a function of swirl ratio: A laboratory investigation. Journal of the Atmospheric Sciences 36, 1755–1776.

Cook, N., Mayne, J., 1980. A refined working approach to the assessment of wind loads for equivalent static design. Journal of Wind Engineering and Industrial Aerodynamics 6, 125–137.

Davison, A.C., Hinkley, D.V., 1997. Bootstrap methods and their application. 1, Cambridge university press.

Gillmeier, S., Sterling, M., Hemida, H., Baker, C., 2018. A reflection on analytical tornado-like vortex flow field models. Journal of Wind Engineering and Industrial Aerodynamics 174, 10–27.

Ginger, J.D., 2000. Internal pressures and cladding net wind loads on full-scale low-rise building. Journal of structural engineering 126, 538–543.

Grazulis, T.P., 2001. The tornado: nature's ultimate windstorm. University of Oklahoma Press.

Haan Jr, F., Balaramudu, V.K., Sarkar, P., 2010. Tornado-induced wind loads on a low-rise building. Journal of structural engineering 136, 106–116.

Haan Jr, F.L., 2017. An examination of static pressure and duration effects on tornado-induced peak pressures on a low-rise building. Frontiers in Built Environment 3, 20.

Haan Jr, F.L., Sarkar, P.P., Gallus, W.A., 2008. Design, construction and performance of a large tornado simulator for wind engineering applications. Engineering Structures 30, 1146–1159.

Hangan, H., 2014. The wind engineering energy and environment (windeee) dome at western university, canada. Wind Engineers, JAWE 39, 350–351.

Hangan, H., Refan, M., Jubayer, C., Parvu, D., Kilpatrick, R., 2017. Big data from big experiments. the windeee dome, in: Whither Turbulence and Big Data in the 21st Century?. Springer, pp. 215–230.

Holmes, J.D., 2007. Wind loading of structures. CRC press.

Hong, H., Huang, Q., Jiang, W., Tang, Q., Jarrett, P., 2021. Tornado wind hazard mapping and equivalent tornado design wind profile for canada. Structural Safety 91, 102078.

Hong, H., Li, S., Mara, T., 2013. Performance of the generalized least-squares method for the gumbel distribution and its application to annual maximum wind speeds. Journal of Wind Engineering and Industrial Aerodynamics 119, 121–132.

Hu, H., Yang, Z., Sarkar, P., Haan, F., 2011. Characterization of the wind loads and flow fields around a gable-roof building model in tornado-like winds. Experiments in fluids 51, 835–851.

Jaffe, A.L., Kopp, G.A., 2021. Internal pressure modelling for low-rise buildings in tornadoes. Journal of Wind Engineering and Industrial Aerodynamics 209, 104454.

Jischke, M., Light, B., 1983. Laboratory simulation of tornadic wind loads on a rectangular model structure. Journal of Wind Engineering and Industrial Aerodynamics 13, 371–382.

Karami, M., Hangan, H., Carassale, L., Peerhossaini, H., 2019. Coherent structures in tornado-like vortices. Physics of Fluids 31, 085118.

Kopp, G.A., Wu, C.H., 2020. A framework to compare wind loads on low-rise buildings in tornadoes and atmospheric boundary layers. Journal of Wind Engineering and Industrial Aerodynamics 204, 104269.

Lieblein, J., 1976. Efficient methods of extreme-value methodology. Technical Report.

van de Lindt, J.W., Pei, S., Dao, T., Graettinger, A., Prevatt, D.O., Gupta, R., Coulbourne, W., 2013. A dual-objective-based tornado design philosophy. Journal of Structural Engineering 139.

Marshall, T.P., 2002. Tornado damage survey at moore, oklahoma. Weather and forecasting 17, 582–598.

Marshall, T.P., McDonald, J., Forbes, G., 2004. The enhanced fujita (ef) scale, in: Preprints, 22nd Conf. on Severe Local Storms, Hyannis, MA, Amer. Meteor. Soc. B.

Mayer, L.J., 2009. Development of a large-scale simulator. Ph.D. thesis.

Mishra, A., James, D., Letchford, C., 2008. Physical simulation of a single-celled tornado-like vortex, part b: Wind loading on a cubical model. Journal of Wind Engineering and Industrial Aerodynamics 96, 1258–1273.

Oh, J.H., Kopp, G.A., Inculet, D.R., 2007. The uwo contribution to the nist aerodynamic database for wind loads on low buildings: Part 3. internal pressures. Journal of wind engineering and industrial aerodynamics 95, 755–779.

Prevatt, D.O., van de Lindt, J.W., Back, E.W., Graettinger, A.J., Pei, S., Coulbourne, W., Gupta, R., James, D., Agdas, D., 2012. Making the case for improved structural design: Tornado outbreaks of 2011. Leadership and Management in Engineering 12, 254–270.

Razavi, A., Sarkar, P.P., 2018. Tornado-induced wind loads on a low-rise building: Influence of swirl ratio, translation speed and building parameters. Engineering Structures 167, 1–12.

Razavi, A., Sarkar, P.P., 2021. Effects of roof geometry on tornado-induced structural actions of a low-rise building. Engineering structures 226, 111367.

Refan, M., Hangan, H., 2018. Near surface experimental exploration of tornado vortices. Journal of Wind Engineering and Industrial Aerodynamics 175, 120–135.

Romanic, D., Refan, M., Wu, C.H., Michel, G., 2016. Oklahoma tornado risk and variability: A statistical model. International journal of disaster risk reduction 16, 19–32.

Roueche, D.B., Prevatt, D.O., Haan, F.L., 2020. Tornado-induced and straight-line wind loads on a low-rise building with consideration of internal pressure. Frontiers in built environment 6, 18.

Sabareesh, G., Cao, S., Wang, J., Matsui, M., Tamura, Y., 2018. Effect of building proximity on external and internal pressures under tornado-like flow. Wind & structures 26, 163–177.

Sabareesh, G.R., Matsui, M., Tamura, Y., 2012. Dependence of surface pressures on a cubic building in tornado like flow on building location and ground roughness. Journal of wind engineering and industrial aerodynamics 103, 50–59.

Sengupta, A., Haan, F.L., Sarkar, P.P., Balaramudu, V., 2008. Transient loads on buildings in microburst and tornado winds. Journal of Wind Engineering and Industrial Aerodynamics 96, 2173–2187.

Simmons, K.M., Sutter, D., Pielke, R., 2013. Normalized tornado damage in the united states: 1950–2011. Environmental Hazards 12, 132–147.

Twisdale, L.A., Banik, S., Mudd, L., Quayyum, S., Liu, F., Faletra, M., Hardy, M., Vickery, P., Levitan, M., Phan, L., 2021. Tornado risk maps for building design: Research and development of tornado hazard risk assessment methodology. National Institute of Standards and Technology .

Wang, J., Cao, S., 2021. Characteristics of tornado wind loads and examinations of tornado wind load provisions in asce 7–16. Engineering Structures 241, 112451.

Wang, J., Cao, S., Pang, W., Cao, J., 2017. Experimental study on effects of ground roughness on flow characteristics of tornado-like vortices. Boundary-Layer Meteorology 162, 319–339.

Wang, J., Cao, S., Pang, W., Cao, J., 2018. Experimental study on tornado-induced wind pressures on a cubic building with openings. Journal of Structural Engineering 144, 04017206.

Wang, M., Cao, S., Cao, J., 2020. Tornado-like-vortex-induced wind pressure on a low-rise building with opening in roof corner. Journal of Wind Engineering and Industrial Aerodynamics 205, 104308.

Williams, J., Dragomirescu, E., 2023. Experimental investigation of tornado induced pressures on residential buildings, in: Canadian Society of Civil Engineering Annual Conference, Springer. pp. 479–488.

Zhang, W., Sarkar, P.P., 2009. Influence of surrounding buildings on tornado-induced wind loads of a low-rise building, in: Proceedings of the 11th Americas conference on wind engineering, San Juan, Puerto Rico.